Molecular Therapy
Nucleic Acids
Original Article

Mir30c Is Involved in Diabetic Cardiomyopathy through Regulation of Cardiac Autophagy via BECN1

Chen Chen,[1,3] Shenglan Yang,[1,2,3] Huaping Li,[1] Zhongwei Yin,[1] Jiahui Fan,[1] Yanru Zhao,[1] Wei Gong,[1] Mengwen Yan,[1] and Dao Wen Wang[1]

[1]Division of Cardiology, Department of Internal Medicine, Institute of Hypertension, Tongji Hospital, Tongji Medical College of Huazhong University of Science and Technology, Hubei Key Laboratory of Genetics and Molecular Mechanisms of Cardiological Disorders (Huazhong University of Science and Technology), Wuhan 430030, China; [2]Department of Cardiology, The First Affiliated Hospital of Chongqing Medical University, Chongqing 400046, China

Multiple factors have been shown to promote the progression of diabetic cardiomyopathy. A link has previously been found between *Mir30* and autophagy in cancer cells and in the heart, but the role of *Mir30* in diabetic heart has not been studied. Using in vitro and in vivo approaches, we found that the depletion of *Mir30c* and induction of BECN1 enhanced autophagy in diabetic (*db/db*) hearts and in cardiomyocytes treated with the fatty acid palmitate. We verified that *Mir30c* repressed *BECN1* expression by direct binding to the *BECN1* 3′ UTRs. *Mir30c* overexpression inhibited the induction of *BECN1* and subsequent autophagy in diabetic hearts and improved cardiac function and structure in diabetic mice. However, these effects were abrogated by *BECN1* overexpression. Similarly, *Mir30c* knockdown resulted in increased BECN1 levels and autophagic flux, aggravating cardiac abnormalities. We also show that SP1, an important transcriptional factor in energy metabolism regulation, is a key upstream activator of *Mir30c* that binds the promoter region of *Mir30c*. Our findings indicate that downregulation of *Mir30c* and subsequent activation of *BECN1* promotes autophagy, contributing to the pathogenesis of diabetic cardiomyopathy. This observation suggests a theoretical ground for developing microRNA-based therapeutics against diabetic cardiomyopathy by inhibiting autophagy.

INTRODUCTION

Over 40 years ago, Rubler et al. described four diabetic patients with congestive heart failure but without obvious coronary diseases.[1] Since then, diabetic cardiomyopathy has been identified as a significant health concern in the rapidly growing population of diabetic patients.

Insulin resistance, hyperglycemia, and obesity are the major characteristics of type 2 diabetes, with a series of downstream events leading to cardiomyocyte death and cardiac dysfunction.[2] Growing evidence indicates that diabetic hearts are characterized by multiple cellular abnormalities, including altered substrate metabolism,[3] increased oxidative stress,[4] mitochondrial dysfunction,[5] and impaired calcium homeostasis.[6] However, the pathogenic molecular mechanisms that affect the heart in type 2 diabetes remain poorly understood. It has been reported that basal constitutive autophagy in the heart plays a cell-protective role, maintaining cell function under stress conditions.[7] Autophagy is the vacuolar degradation of intracellular components, e.g., long-lived or damaged proteins and organelles, that underpins cell survival.[8] However, excessive autophagy can be detrimental, leading to non-apoptotic programmed cell death.[9, 10] A recent study revealed a novel role of autophagy in the pathogenesis of diabetic cardiomyopathy by demonstrating that the activation of myocardial autophagy in fructose-fed mice was associated with increased production of reactive oxygen species (ROS), fibrosis, and cardiomyocyte loss, contributing to cardiac insulin resistance.[11]

MicroRNAs (miRNAs) are a class of recently discovered, endogenous, single-stranded, non-coding RNAs 22–23 nt long.[12] These molecules modulate gene expression at the post-translational level.[13] Emerging evidence has implicated cardiac-enriched miRNAs in heart diseases.[14] Many miRNAs that are differentially expressed during disease repress or promote key target genes, regulate cell signaling, and modulate pathogenic processes. *Mir148a*, which is enriched in human and mouse hepatic tissues, and differentially expressed in the livers of mice fed a high-fat diet (HFD), regulates cholesterol metabolism via inhibiting low density lipoprotein receptor (LDLR) expression.[15] However, little is known about the role of miRNAs in diabetes and in the cardiovascular complications of this disease. To date, only few have been identified as potential key regulators of diabetic complications in the heart.[16]

Previously, Zhu et al. reported a link between *Mir30*, a miRNA family highly expressed in cardiomyocytes, and autophagy.[17] They found that the initiator of autophagy Beclin-1 (*BECN1*) was a *Mir30a* target

Received 16 January 2017; accepted 17 March 2017;
http://dx.doi.org/10.1016/j.omtn.2017.03.005.

[3]These authors contributed equally to this work

Correspondence: Dao Wen Wang, Division of Cardiology, Department of Internal Medicine, Tongji Hospital, Tongji Medical College, Huazhong University of Science and Technology, 1095 Jiefang Avenue, Wuhan 430030, China.
E-mail: dwwang@tjh.tjmu.edu.cn

This is an open access article under the CC BY-NC-ND license (http://creativecommons.org/licenses/by-nc-nd/4.0/).

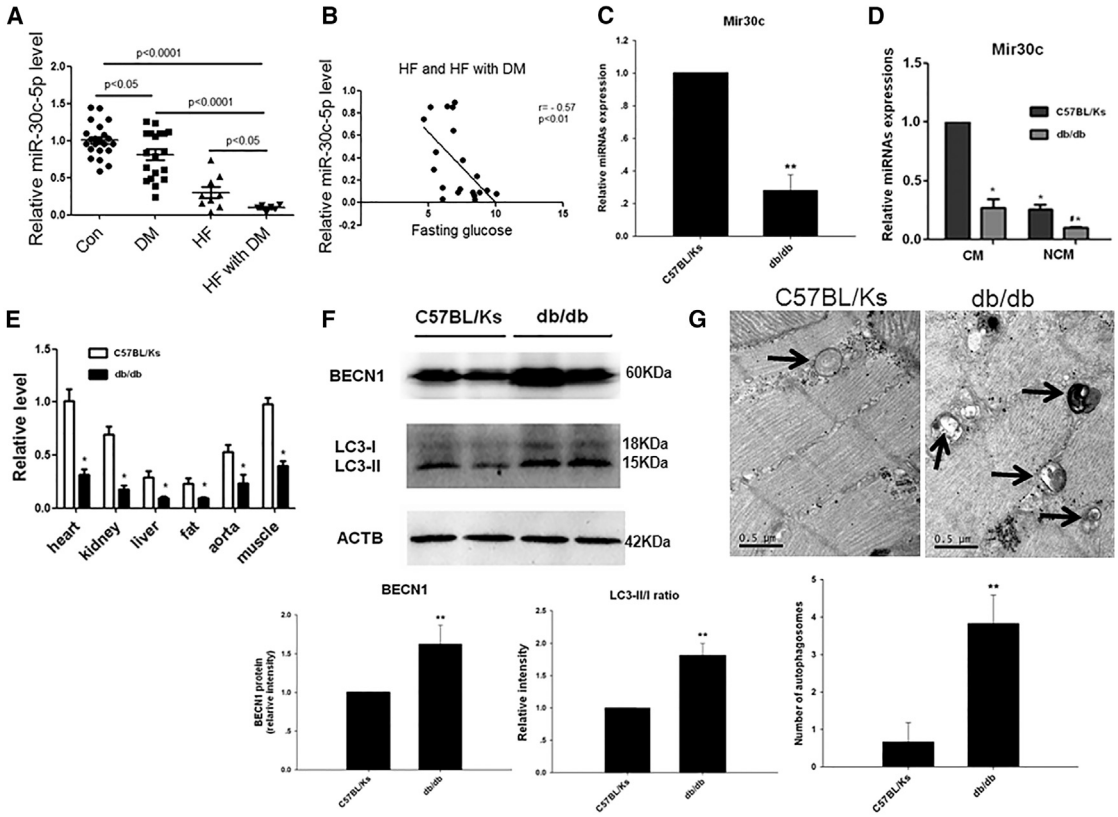

Figure 1. *Mir30c* Is Downregulated and Autophagy Is Induced in Diabetic Mouse Hearts

(A) Relative circulating miRNA levels in patients. (B) The correlation between circulating Mir30c levels and fasting glucose. Relative *Mir30c* expression was determined by qRT-PCR in the heart (C), CMs and NCMs (D), and various organs (E) in 24-week-old animals. (F) Western blotting detection (left) and quantification (middle and right) of the cardiac autophagy-related proteins BECN1 and LC3. ACTB was used as an internal control. (G) Representative autophagic vacuoles from cardiac tissues (arrows) analyzed by transmission electron microscopy (magnification ×38,000). Data are expressed as mean ± SEM (n = 8). For all panels, *p < 0.05 versus C57BL/Ks; **p < 0.01 versus C57BL/Ks. Data are representative of three independent experiments.

and *Mir30a* overexpression decreased autophagic activity in cancer cells.[18] *Mir30* was also shown to mediate angiotensin-II-induced myocardial hypertrophy by regulating autophagy.[19] Downregulated *Mir30c* enhanced myocardial matrix remodeling in pathological left ventricular hypertrophy (LVH).[20]

Taken together, these previous findings suggest a possible regulatory association of *Mir30c*, autophagy, and diabetic cardiomyopathy. We therefore asked whether *Mir30c* is involved in the pathology of diabetic cardiomyopathy in type 2 diabetes and whether *Mir30c* contributes to diabetic cardiomyopathy by regulating autophagy. Herein, we investigate this hypothesis using in vivo and in vitro models.

RESULTS

Mir30c Is Downregulated and Autophagy Is Induced in Diabetic Hearts

First, we determined *Mir30c* levels in plasma taken from 28 healthy controls, 26 patients with diabetes, 22 patients with chronic heart failure, and 15 patients with both diabetes and chronic heart failure (see Table S1 for details of the participants). Plasma *Mir30c* levels were reduced in the patients with disease (Figure 1A). Consistently, plasma *Mir30c* levels were negatively correlated with plasma glucose levels in patients with chronic heart failure (Figure 1B).

To further investigate the association of *Mir30c* with the pathogenesis of diabetic heart failure, we measured *Mir30c* expression in the myocardium of diabetic cardiomyopathy db/db mice and non-diabetic control C57BL/Ks mice. It was reported that diabetic db/db mice developed severe diabetes by 8 weeks of age and exhibited cardiomyopathy, as evidenced by signs of cardiac hypertrophy.[21] We observed a significant reduction in the expression of *Mir30c* in the hearts of 24-week-old db/db mice compared with C57BL/Ks controls, especially in isolated cardiomyocytes (Figures 1C, 1D, S1A, and S1B). *Mir30c* was abundantly expressed in the cardiac tissue and cardiomyocytes compared with other organs (Figures 1E and S1C–S1E).

BECN1 is a well-conserved protein and plays a central role during the autophagy process. In db/db hearts, levels of BECN1 protein were

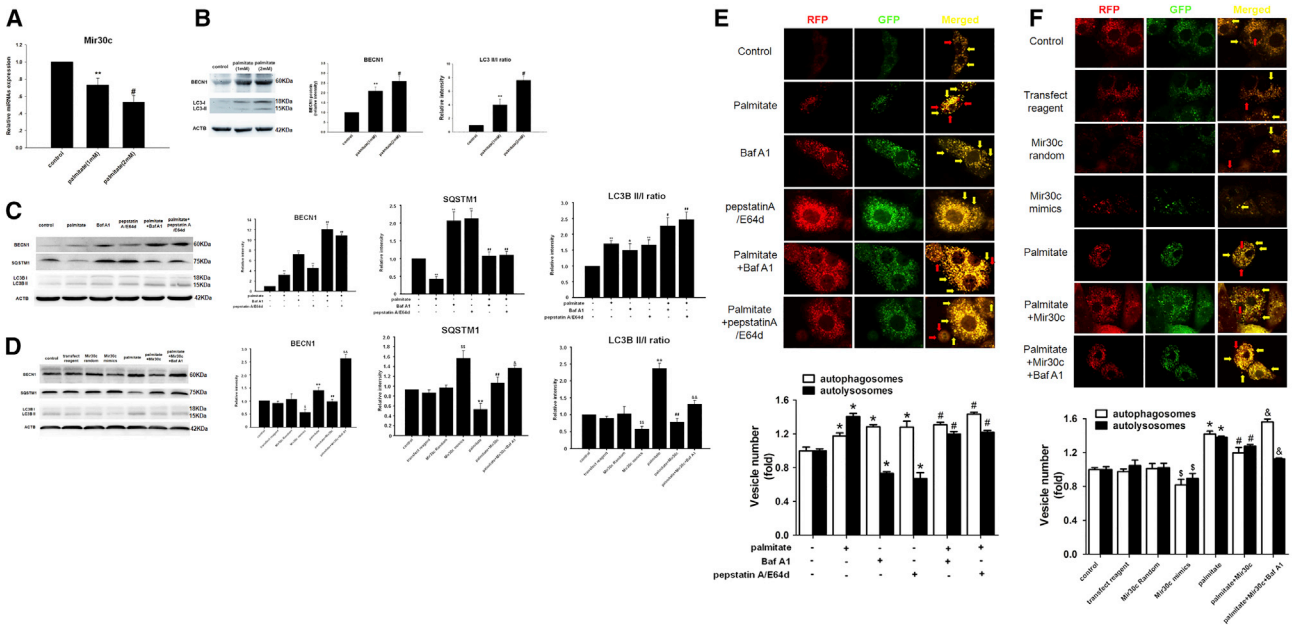

Figure 2. High FFA Concentrations Inhibit *Mir30c* Expression and Enhance Autophagy in Cultured H9c2 Cardiac Cells

H9c2 cells were analyzed after 48-hr treatment with different concentrations of palmitate (1 mM or 2 mM) and *Mir30c* mimics (100 nM) in the presence or absence of 2 hr Baf A1 (10 nM), pepstatin A (10 μg/mL), or E64d (10 μg/mL). (A) Relative *Mir30c* expression in H9c2 cells treated with palmitate, as determined by qRT-PCR. (B–D) Levels of BECN1 and LC3 (B) and BECN1, LC3, and SQSTM1 (C and D) were determined in cell lysates by western blotting. ACTB was used as an internal control. (E and F) Live-cell imaging of H9c2 cells transfected with Ad-mRFP-GFP-LC3 (1,000× magnification). Autophagosomes are labeled both with GFP and mRFP and appear yellow in the merged image (yellow arrow indicated). Autolysosomes are labeled with mRFP only and appear red in the merged image (red arrow indicated). Data are expressed as mean ± SEM. For all panels, $^{*}p < 0.05$ versus control, $^{**}p < 0.01$ versus control, $^{\#}p < 0.05$ versus palmitate (1 mM), $^{\#\#}p < 0.01$ versus palmitate (1 mM), $^{\$}p < 0.05$ versus *Mir30c* Random, $^{\$\$}p < 0.01$ versus *Mir30c* random, $^{\&}p < 0.05$ versus palmitate + *Mir30c*, and $^{\&\&}p < 0.01$ versus palmitate + *Mir30c*. Data are representative of three independent experiments.

significantly increased compared with normal controls (Figure 1F). During autophagy, the autophagy-related protein LC3-I is converted to lipidated LC3-II; hence, the ratio of these two compounds has been identified as a marker of autophagy. Notably, we found that the LC3-II:LC3-I (LC3-II:I) ratio was greater in the hearts of db/db mice than in the hearts of control mice (Figure 1F). The increased LC3-II:I ratio indicated that diabetes induced both autophagosome synthesis and degradation. In addition, we directly quantified autophagosomes using electron microscopy. These double-membrane vesicles are indicative of autophagy. Significantly, four times as many autophagosomes were observed in db/db hearts than in C57BL/Ks mice detected by electron microscopy (Figure 1G).

High Free Fatty Acid Concentrations Inhibit *Mir30c* Expression and Enhance Autophagy in Cultured H9c2 Cardiac Cells

To elucidate the role of autophagy in diabetic cardiomyopathy under high plasma free fatty acid (FFA) conditions, which is a key characteristic of type 2 diabetes, we established a cell culture model of lipotoxicity by culturing H9c2 rat cardiac cells in high-FFA medium in vitro. Compared with untreated controls, high FFA concentrations led to a decrease in expression of *Mir30c* (Figure 2A). In contrast, BECN1 and LC3-II:I protein levels significantly increased in an FFA-concentration-dependent manner (Figure 2B).

Inhibitors of autophagic degradation, bafilomycin A1 (Baf A1) and pepstatin A with E64d, were added to measure the autophagic flux. Both autophagy inhibitors led to elevated LC3-II:I ratios, indicating that they blocked autophagosomal degradation (Figure 2C). The increased LC3-II:I ratio in palmitate-treated cells (compared with the control) indicated that palmitate induced both autophagosome synthesis and degradation. Moreover, in the presence of either autophagy inhibitor, the LC3-II:I ratio was further increased by the addition of palmitate, implying that palmitate induced autophagosome generation. Similarly, FFA and autophagy inhibitors exerted same effects on protein expression of BECN1. On the other hand, a palmitate-induced decrease in SQSTM1 levels suggested autophagy activation, with autophagy inhibitors exerting an opposite effect (Figure 2C). In addition to LC3, SQSTM1 is also a protein marker of autophagy. SQSTM1 and SQSTM1-bound polyubiquitinated proteins become incorporated into the completed autophagosome and are degraded in autolysosomes, thus serving as an index of autophagic degradation. Taken together, these results show that FFA stimulation of H9c2 cells results in an increase in autophagic flux (Figure 2C). Similar effects were observed in palmitate-treated H9c2 cells incubated for different time periods with autophagy inhibitors (Figure S2).

To investigate the effects of *Mir30c* on autophagy, *Mir30c* mimics were transfected in vitro. Exogenous *Mir30c* decreased palmitate-enhanced

BECN1 and LC3-II:I levels, while Baf A1 counteracted this inhibition (Figure 2D). In contrast, exogenous *Mir30c* increased palmitate-reduced SQSTM1 levels, and the addition of Baf A1 led to an even higher increase in SQSTM1 levels. These data suggested that the FFA-enhanced autophagic flux was alleviated by *Mir30c* treatment (Figure 2D).

Next, to monitor autophagic flux, we used an adenovirus that constitutively expresses monomeric red fluorescent protein (mRFP)-GFP tandem fluorescently tagged LC3 (Ad-mRFP-GFP-LC3). In this system, autophagosomes produce both mRFP and GFP signals, whereas autolysosomes produce only mRFP signal because of GFP quenching in the acidic lysosomal environment. Therefore, in a merged fluorescence image, yellow puncta correspond to autophagosomes and red puncta indicate autolysosomes, thereby allowing us to determine autophagic flux. As shown in Figure 2E, palmitate increased both the yellow and red puncta numbers, whereas cells treated with Baf A1 or pepstatin A/E64d predominantly contained yellow puncta. Consistently with data presented in Figure 2C, fewer red and more numerous yellow puncta were observed in the presence of either inhibitor plus palmitate compared with palmitate-only-treated cells, reinforcing the notion that palmitate stimulates autophagic flux (Figure 2E). Furthermore, exogenous *Mir30c* somewhat inhibited the palmitate-induced increase in yellow and red vesicle number, whereas Baf A1 enhanced the number of yellow puncta but reduced the number of red puncta (Figure 2F). Taken together, these results indicate that palmitate stimulates autophagic flux and exogenous *Mir30c* inhibits these palmitate-induced changes.

All these results were consistent with our observations in the hearts of db/db mice, suggesting that the regulation of *Mir30c* and autophagy might play a role in the pathological processes of diabetic cardiomyocytes.

BECN1 Is a Direct Target of *Mir30c*

We first used a bioinformatics approach using TargetScan software to predict the target genes of *Mir30c*. Notably, BECN1 was identified as a potential *Mir30c* target (Figure 3A). By aligning human, rat, and mouse BECN1 3′ UTRs, we noted that the predicted *Mir30c* binding sites were highly conserved ($\geq$75%), which suggested that these sites may be important for *Mir30c* regulation of BECN1 expression (Figure 3A).

Then we transfected H9c2 cells with *Mir30c* mimics. Western blotting revealed that compared with *Mir30c* control-transfected cells, *Mir30c* mimics significantly reduced BECN1 levels (Figure 3B), but not the levels of other autophagy-related proteins (Figure S3). To verify a direct repression of BECN1 translation by *Mir30c*, we then cloned the BECN1 3′ UTR (wild-type [WT] and a mutated seed region sequence) into pMIR-report vector, a luciferase expression plasmid, resulting in plasmids pMIR-BECN1-3′ UTR and pMIR-mut-BECN1-3′ UTR (Figure 3C). We found that co-transfection of pMIR-BECN1 3′ UTR with the *Mir30c* mimics resulted in a significant decrease in luciferase activity compared with pMIR-BECN1 3′ UTR/control miRNA transfection (Figure 3D). However, the repressive effect of *Mir30c* mimics was abrogated by mutating the BECN1 3′ UTR (Figure 3D). Furthermore, we found that the protective effect of BECN1 knockdown on cell survival in palmitate-treated H9c2 cells was replicated by *Mir30c* overexpression, as indicated by higher cell viability compared with palmitate-only cells (Figure 3E). BECN1 knockdown or exogenous *Mir30c* expression enhanced the proliferation of H9c2 cells (Figure 3F). In contrast, *Mir30c* and si-BECN1 treatment decreased the H9c2 cell apoptosis induced by palmitate (Figure 3G). Similarly, *Mir30c* and si-BECN1 treatment inhibited palmitate-induced caspase activity in H9c2 cells (Figure 3H). Overall, these results suggest that *Mir30c* regulates BECN1 translation by binding to its 3′ UTR, which may protect cardiomyocytes to survive.

Overexpression of *Mir30c* Rescues Cardiac Dysfunction in db/db Mice

We investigated the effect of recombinant adeno-associated virus 9 (rAAV9)-mediated *Mir30c* overexpression on cardiac dysfunction in vivo in db/db mice. qRT-PCR analyses revealed that overexpression of *Mir30c* in the heart was induced in a time-dependent manner (Figure S4), and *Mir30c* did not affect cardiac functions of WT C57BL/Ks mice under normal conditions without any stress (Table S2). First, we performed a titration with three different doses of WT BECN1. BECN1 expression was subsequently rescued in a dose-dependent manner (Figure S5A). Then, we chose the intermediate (1×10^{11}) virion particle dose for further experiments, as it restored BECN1 expression to normal levels. rAAV-*Mir30c* administration resulted in enhanced *Mir30c* overexpression in the heart, whereas rAAV-anti-*Mir30c* inhibited *Mir30c* expression (Figure 4A). Moreover, compared with other organs, the rAAV-transduced *Mir30c* was predominantly expressed in the heart, especially in cardiomyocytes (Figures 4B and 4C).

Next, we performed echocardiographic and hemodynamic analyses to examine the effects of rAAV treatments on cardiac function in db/db mice. The experiments revealed that db/db mice developed cardiac hypertrophy and diabetic cardiomyopathy, as shown by increased left ventricular (LV) mass, reduced fractional shortening (FS), decreased LV ejection fraction (LVEF), and reduced dp/dt_{max}, (the peak instantaneous rate of LV pressure increase) and dp/dt_{min} (the peak instantaneous rate of LV pressure decline) (Figures 4D–4F; Table S3). As determined by echocardiographic analyses, overexpression of *Mir30c* in db/db mice significantly increased LVEF and FS values and reduced LV mass compared with control diabetic hearts (Figures 4D and 4E). In contrast, knocking down *Mir30c* by rAAV-anti-*Mir30c* administration reduced LVEF and FS (Figures 4D and 4E). Notably, BECN1 overexpression counteracted the protective effects of *Mir30c* and exacerbated cardiac dysfunction in db/db mice, as indicated by decreased LVEF and FS values, and increased LV mass (Figures 4D and 4E). Echocardiographic characteristics of C57BL/Ks mice and db/db mice that underwent various treatments are given in Table S3.

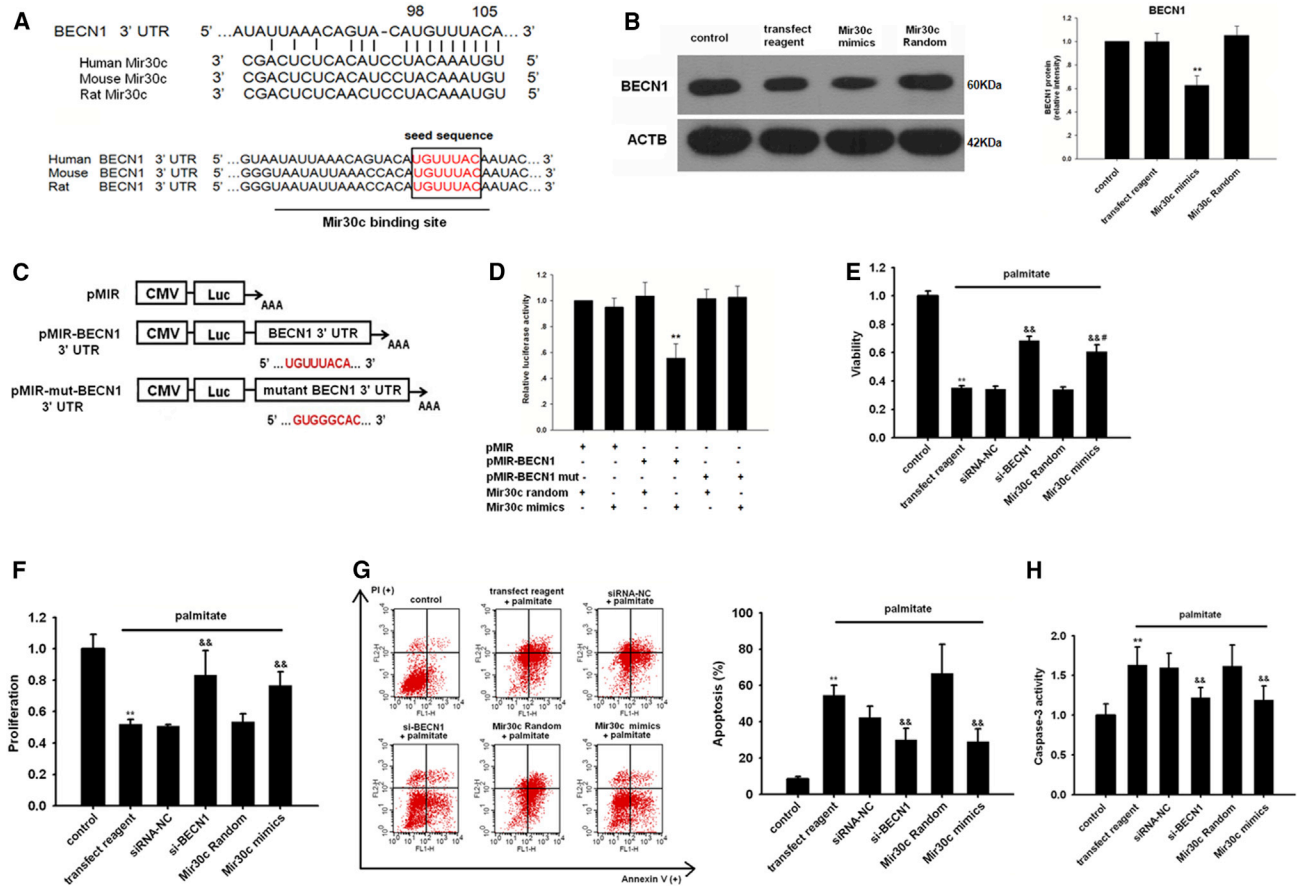

Figure 3. BECN1 Is a Direct Target of *Mir30c*

(A) Sequence alignment of *Mir30c* and BECN1 3′ UTR from different species. (B) The effect of *Mir30c* on the BECN1 protein levels in H9c2 cells was determined by western blotting. **$p < 0.01$ versus *Mir30c* random. (C) A schematic diagram of luciferase reporter plasmids pMIR-BECN1 3′ UTR-WT and pMIR-mut-BECN1 3′ UTR, with the potential *Mir30c* target site on BECN1 3′ UTR shown in red. (D) Regulation of BECN1 via *Mir30c*-targeting of BECN1 3′ UTR was determined with luciferase reporter assays in HEK293 cells. **$p < 0.01$ versus BECN1 3′ UTR + *Mir30c* random. H9c2 cells were treated with various RNA constructs and their viability (E), proliferation (F), and apoptosis (G and H) were determined by CCK8 assay, BrdU incorporation assay, and Annexin V/PI and caspase-3 activity assay, respectively, as described in the Materials and Methods. **$p < 0.01$ versus control, $^{\&\&}p < 0.01$ versus palmitate + transfection reagent, and $^{\#}p < 0.05$ versus palmitate + si-BECN1. Data are expressed as mean ± SEM and are representative of three independent experiments.

Hemodynamics analysis revealed elevated dp/dt_{max} and dp/dt_{min} in *Mir30c*-overexpressing mice (Figure 4F). In contrast, *Mir30c* knockdown decreased dp/dt_{max} and dp/dt_{min}, suggesting that *Mir30c* improves cardiac function in diabetic cardiomyopathy; BECN1 abolished these positive effects of *Mir30c* (Figure 4F). In addition, neither the Millar system nor echocardiographic examinations indicated differences in the preload $volume_{max}$ between the tested groups (Figures S5B and S5C). Afterload Ea was increased in the db/db groups compared with the C57BL/Ks controls but remained unchanged among db/db groups, indicating reduced arterial elastance (Figure S5D).

We overexpressed the BECN1 coding domain sequence (CDS) region and 3′ UTR (WT or mutated) in db/db mice using the rAAV system (Table S4). Compared with rAAV-*Mir30c* treatment, rAAV-*Mir30c* + rAAV-BECN1 3′ UTR mut (mutated) treatment significantly decreased cardiac functions, whereas rAAV-*Mir30c* + rAAV-BECN1 3′ UTR WT administration resulted in no significant changes. Moreover, decreased cardiac function was observed in the rAAV-miR-random + rAAV-BECN1 3′ UTR WT group compared with rAAV-miR-random group.

We also determined cardiomyocyte size, as an indicator of hypertrophy, and observed that rAAV-*Mir30c* treatment repressed diabetes-associated cell enlargement. However, this repression was reversed by simultaneous overexpression of BECN1; the repression was also not observed after anti-*Mir30c* administration (Figure 4G). Masson and Sirius red staining revealed mild cardiac fibrosis in db/db mice compared with the C57BL/Ks control mice (Figures 4H and 4I). *Mir30c* administration alleviated cardiac fibrosis. BECN1

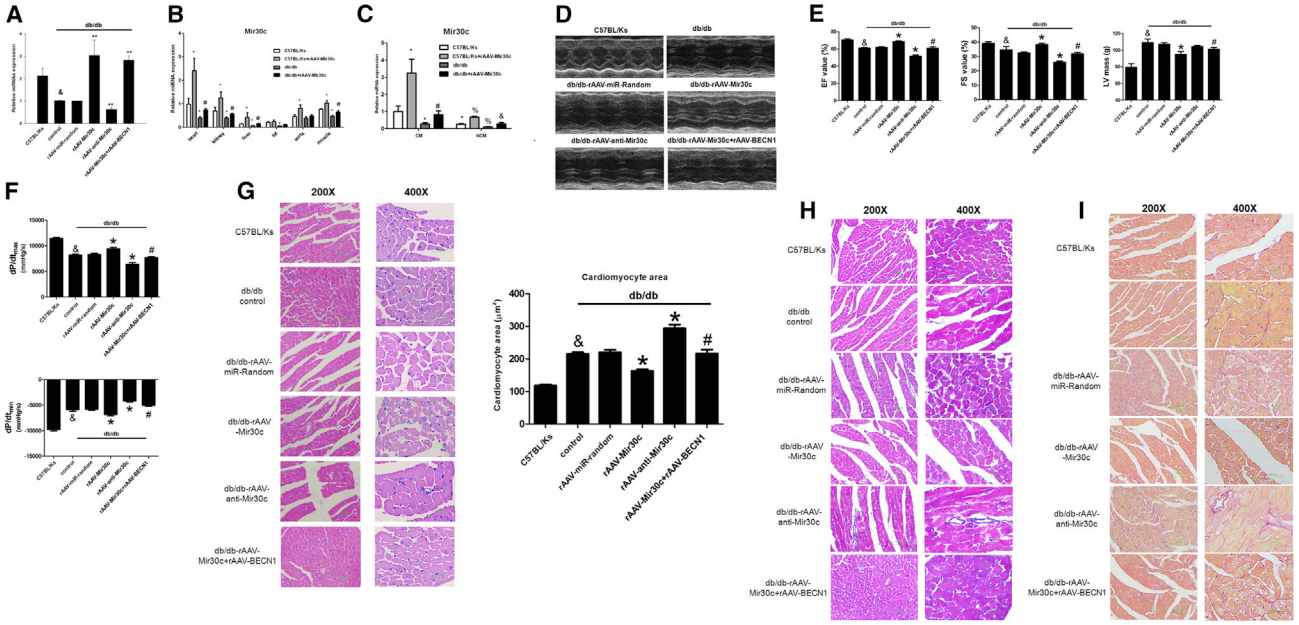

Figure 4. *Mir30c* Overexpression Relieves Cardiac Dysfunction in db/db Mice

Animals (24-week-old db/db mice and C57BL/Ks control mice) were analyzed after treatment with recombinant adeno-associated viruses (rAAVs). (A–C) Relative expression of *Mir30c* was determined by qRT-PCR. (A) Cardiac expression of *Mir30c* in rAAV-treated mice. $^{\&}p < 0.05$ versus C57BL/Ks and $^{**}p < 0.01$ versus db/db control. (B) Relative expression of *Mir30c* in different organs. $^{*}p < 0.05$ versus C57BL/Ks and $^{\#}p < 0.05$ versus db/db. (C) Relative expression of *Mir30c* in isolated CMs and NCMs. $^{*}p < 0.05$ versus C57BL/Ks CM, $^{\#}p < 0.05$ versus db/db CM, $^{\%}p < 0.05$ versus C57BL/Ks NCM, and $^{\&}p < 0.05$ versus db/db NCM. (D and E) Echocardiographic analysis of db/db mice and C57BL/Ks controls. EF% (ejection fraction), FS% (fractional shortening), and LV masses were quantitatively analyzed. (F) Hemodynamic analysis of db/db mice and C57BL/Ks controls. dp/dt_{max}, peak instantaneous rate of LV pressure increase; dp/dt_{min}, peak instantaneous rate of LV pressure increase decline. (G) CM visualization and CM size quantitation following various treatments. $^{\&}p < 0.05$ versus C57BL/Ks, $^{*}p < 0.05$ versus db/db control, $^{**}p < 0.01$ versus db/db control, and $^{\#}p < 0.05$ versus db/db rAAV-*Mir30c*. (H) Cardiac fibrosis, as determined by Masson staining. (I) Cardiac fibrosis, as determined by Sirius red staining. Data are expressed as mean ± SEM (n = 8) and are representative of three independent experiments.

overexpression inhibited the anti-fibrosis effects of *Mir30c*, whereas anti-*Mir30c* treatment aggravated cardiac fibrosis in db/db mice (Figures 4H and 4I).

Taken together, our data suggest that *Mir30c* alleviates the cardiac dysfunction associated with diabetic cardiomyopathy in db/db mice, and that this effect can be counteracted by BECN1.

Mir30c Downregulates BECN1, Protecting db/db Hearts from Excessive Autophagy

Next, we tested whether *Mir30c* repression of BECN1 inhibits excessive autophagy in db/db mice. Western blot revealed increased BECN1 levels, increased LC3-II:I ratio, decreased SQSTM1 levels, and more autophagosomes in db/db hearts compared with C57BL/Ks controls, indicating enhanced autophagy (Figures 5A and 5B).

Overexpression of *Mir30c* in db/db mice resulted in decreased BECN1 levels and LC3-II:I ratio and increased SQSTM1 levels compared with the untreated db/db mice, reflecting inhibition of autophagic flux. By contrast, anti-*Mir30c* treatment resulted in the opposite effects, indicating accelerated autophagy (Figure 5A). Furthermore, overexpression of BECN1 reversed the *Mir30c*-depressed autophagy, as indicated by the increased LC3-II:I ratio in these mice (Figure 5A). Fewer autophagic vacuoles were observed with electron microscopy in *Mir30c*-overexpressing db/db mice, and knockdown of *Mir30c* by rAAV-anti-*Mir30c* resulted in more autophagosomes compared with control db/db mice (Figure 5B). Consistently with western blot (Figure 5A), overexpression of BECN1 abrogated the *Mir30c*-induced reduction of autophagic vesicle numbers (Figure 5B).

Next, mice were transfected with a GFP-LC3 plasmid to monitor autophagosome formation in the heart. We observed that GFP-LC3-positive vesicles were rare in the hearts of control C57BL/Ks mice but significantly increased in db/db mice. Compared with db/db mice, the inhibition of GFP-LC3-positive vesicle formation in rAAV-*Mir30c*-treated db/db mice was reversed by BECN1 overexpression, whereas rAAV-anti-*Mir30c* enhanced the formation of GFP-LC3-positive vesicles beyond control (db/db untreated mice) levels. These data indicate that diabetes-induced autophagosome formation is suppressed by *Mir30c* inhibition of BECN1 (Figure S6).

Interestingly, as measured by LC3 in situ staining, *Mir30c* overexpression in vivo was accompanied by decreased cardiac LC3 levels, and this effect was attenuated by BECN1 overexpression. On the other

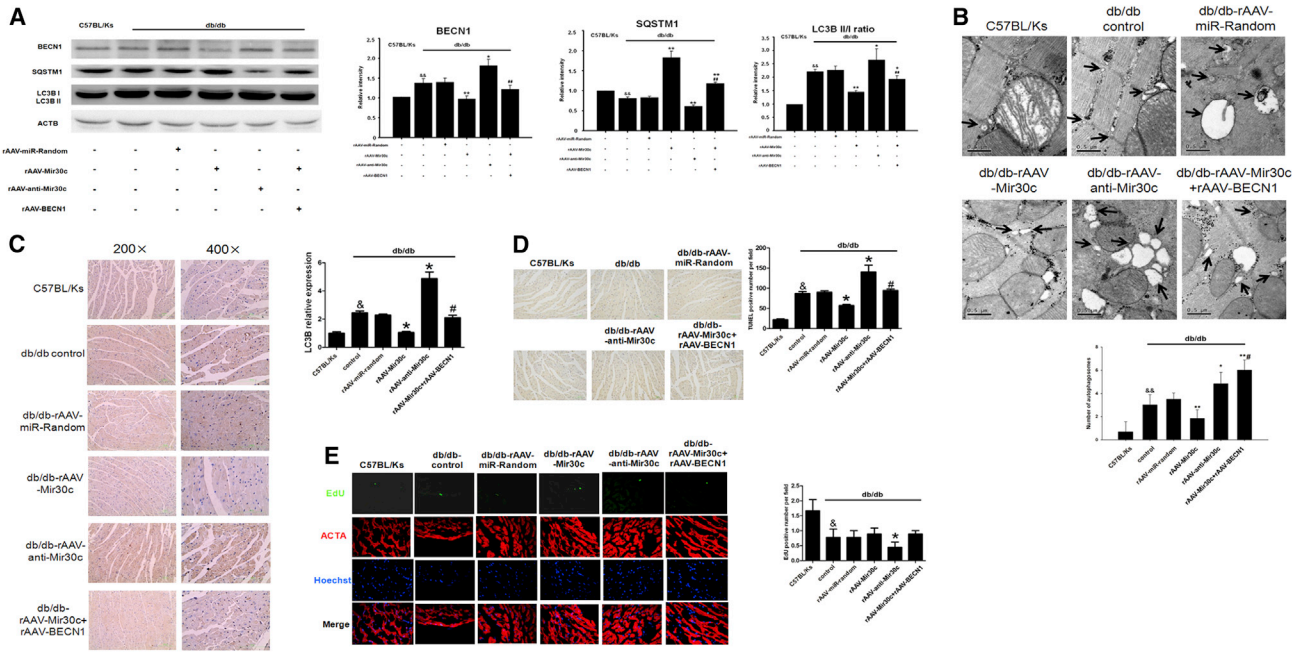

Figure 5. *Mir30c* Downregulates BECN1, Protecting db/db Hearts from Excessive Autophagy

(A) Mice were treated with different RNA constructs, and BECN1, SQSTM1, and LC3 protein levels were determined by western blotting, with ACTB as an internal control. Protein band intensity in C57BL/Ks was set as 1, and relative protein intensities are presented as fold changes. (B) Autophagosomes (arrows) in mouse cardiac tissues were analyzed by transmission electron microscopy and quantified per field. (C) Cardiac LC levels were assessed by immunohistochemistry. (D) Cardiac apoptosis was examined with TUNEL assay (200× magnification). (E) Cardiac proliferation was determined by EdU staining (600× magnification). In all panels, data are expressed as mean ± SEM (n = 8). $^{\&}p < 0.05$ versus C57BL/Ks, $^{\&\&}p < 0.01$ versus C57BL/Ks, $^{*}p < 0.05$ versus db/db control, $^{**}p < 0.01$ versus db/db control, $^{\#}p < 0.05$ versus db/db rAAV-*Mir30c*, and $^{\#\#}p < 0.01$ versus db/db rAAV-*Mir30c*. Data are representative of three independent experiments.

hand, rAAV-anti-*Mir30c* treatment led to increased LC3 expression compared with db/db control mice (Figure 5C). Furthermore, TUNEL assays revealed that BECN1 overexpression reversed the reduced apoptosis effect of *Mir30c* overexpression in heart tissues in db/db mice (as indicated by increased numbers of TUNEL-positive cells; Figure 5D). Moreover, 5-ethynyl-2'-deoxyuridine (EdU) in situ staining demonstrated that anti-*Mir30c* expression in vivo inhibited cardiomyocyte proliferation in db/db mice, as indicated by fewer EdU-positive cardiomyocytes compared with db/db mice (Figure 5E).

Together, our data show that *Mir30c* overexpression silences BECN1 and inhibits BECN1-activated autophagy, contributing to the protection of cardiac function in diabetic db/db mice. However, the loss of *Mir30c* leads to induced BECN1 expression, enhanced autophagy, and therefore contributes to diabetic heart pathology.

SP1 Regulates *Mir30c* In Vitro

Using bioinformatics, we identified SP1, an important transcriptional factor in energy metabolism regulation, as the most promising regulator of *Mir30c* promoter. To modulate SP1 expression, H9c2 cells were transfected with an SP1-specific small interfering RNA (si-SP1). We observed a marked decrease in *Mir30c* expression upon si-SP1 transfection, suggesting that *Mir30c* is indeed regulated by SP1 (Figure 6A). We therefore cloned the promoter region of *Mir30c* into a pGL3 vector. Luciferase activity, as controlled by the *Mir30c* promoter constructs, was significantly reduced relative to the small interfering RNA (siRNA) negative control, indicating that SP1 acted via the promoter region of *Mir30c* to modulate *Mir30c* expression (Figure 6B). Additionally, western blot and qRT-PCR analyses revealed that downregulation of SP1 in cardiac cells in vitro resulted in enhanced BECN1 expression (Figures 6C and 6D). Next, we performed chromatin immunoprecipitation (ChIP) assays in HEK293 cells and observed that endogenous SP1 was able to directly bind to the −500-bp to 0-bp region upstream of *Mir30c* (Figure 6E). Overexpression of SP1 in H9c2 cells reversed the palmitate-induced *Mir30c* reduction and BECN1 stimulation at both the mRNA and protein levels (Figures 6F and 6G).

Downregulation of SP1 in db/db Hearts Contributes to *Mir30c* Loss and the Resultant BECN1 Increase Promotes Excessive Autophagy

After verifying that *Mir30c* was positively regulated by SP1, we aimed to determine whether the depletion of *Mir30c* in db/db hearts was also SP1 regulated. We discovered that both SP1 mRNA (Figure 6H) and protein levels (Figure 6I) were reduced in db/db hearts in comparison with the C57BL/Ks controls, in agreement with previous studies; in contrast, BECN1 protein levels were increased in db/db hearts (Figure 6J). Meanwhile, decreased SQSTM1 and increased LC3 levels

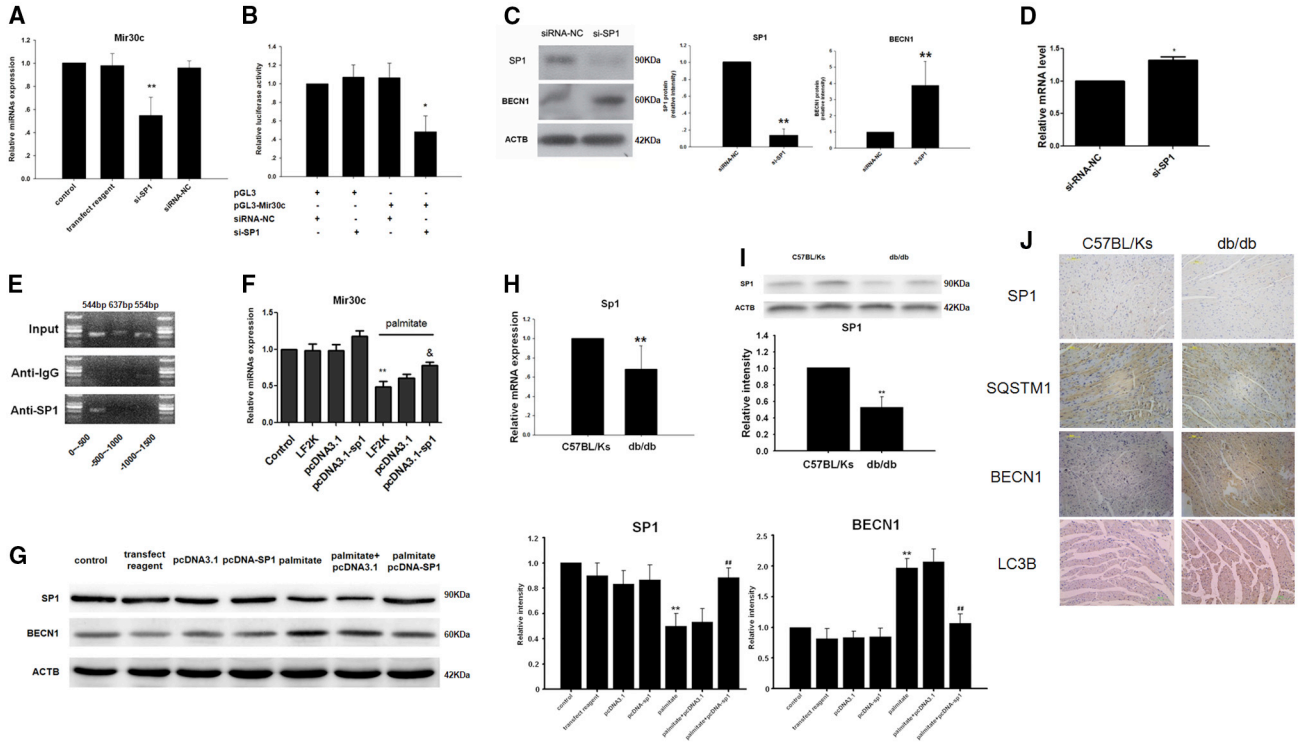

Figure 6. SP1 Regulates *Mir30c* In Vitro

(A) Relative *Mir30c* expression in H9c2 cells treated with siRNA was determined by qRT-PCR. $^{**}p < 0.01$ versus siRNA-NC. (B) Regulation of *Mir30c* expression by SP1 was analyzed by luciferase assays. $^{*}p < 0.05$ versus pGL3-*Mir30c* + siRNA-NC. (C) BECN1 and SP1 protein levels in H9c2 cells transfected with si-SP1, as determined by western blotting. ACTB was used as an internal control. (D) Relative mRNA expression levels of BECN1 in H9c2 cells transfected with si-SP1. Gene expression was analyzed by qRT-PCR. $^{*}p < 0.05$ versus siRNA-NC and $^{**}p < 0.01$ versus siRNA-NC. (E) ChIP assays were performed with HEK293 cells. (F) Relative *Mir30c* expression in vitro, as determined by qRT-PCR. $^{**}p < 0.01$ versus control and $^{\&}p < 0.05$ versus palmitate + LF2K. (G) Relative protein levels of BECN1 and SP1 invitro analyzed by western blotting. ACTB was used as an internal control. $^{**}p < 0.01$ versus control and $^{\#\#}p < 0.01$ versus palmitate. (H) Relative Sp1 mRNA levels in animal hearts were determined by qRT-PCR. Gapdh was used as an internal control. (I) Relative Sp1 protein levels in animal hearts were detected by western blotting and ACTB was used as an internal control. Data are expressed as mean ± SEM (n = 8). $^{**}p < 0.01$ versus C57BL/Ks. (J) SP1, SQSTM1, BECN1, and LC3B proteins in rodent hearts were detected by immunohistochemistry (200× magnification). In all panels, data are representative of three independent experiments.

indicated that autophagy played a role in diabetic cardiomyopathy (Figure 6J). The results support our hypothesis that SP1 downregulation contributes to *Mir30c* downregulation in db/db hearts.

Collectively, our results demonstrate that *Mir30c* is decreased and BECN1-activated autophagy is induced in db/db mice.

DISCUSSION

In response to the characteristically high levels of FFAs in type 2 diabetes, high FFA levels have been shown to promote the progression of diabetic cardiomyopathy via multiple factors.[22] In the present study, we conclude that in db/db hearts, *Mir30c* reduction caused by SP1 downregulation increases BECN1 expression, promoting excessive autophagy, and contributing to the pathology of diabetic cardiomyopathy (Figure 7).

Recently, the *Mir30* family was reported to be among the most highly expressed group of miRNAs in cardiomyocytes, which is consistent with our conclusions.[20] Duisters et al. showed that *Mir30c* levels were decreased in animal models and human LVH, resulting in increased levels of connective tissue growth factor and leading to myocardial matrix remodeling.[20] In another study, downregulation of *Mir30* was shown to mediate angiotensin-II-induced myocardial hypertrophy by regulating autophagy.[19] These studies demonstrated that *Mir30* family levels substantially decreased during LVH, leading to heart failure. However, the upstream regulator responsible for *Mir30* downregulation in the course of pathological hypertrophy was not known.

In our present study, we focused on diabetic cardiomyopathy. Consistent with previous studies, we found that depletion of *Mir30c* in diabetic hearts and the relative lack of *Mir30c* was associated with cardiac abnormalities, enhancing the link between *Mir30c* downregulation and LVH. We also showed that high FFA levels decreased *Mir30c* levels in cardiomyocytes. Other mechanisms may also be involved in *Mir30* loss in LVH. However, considering that FFA levels are

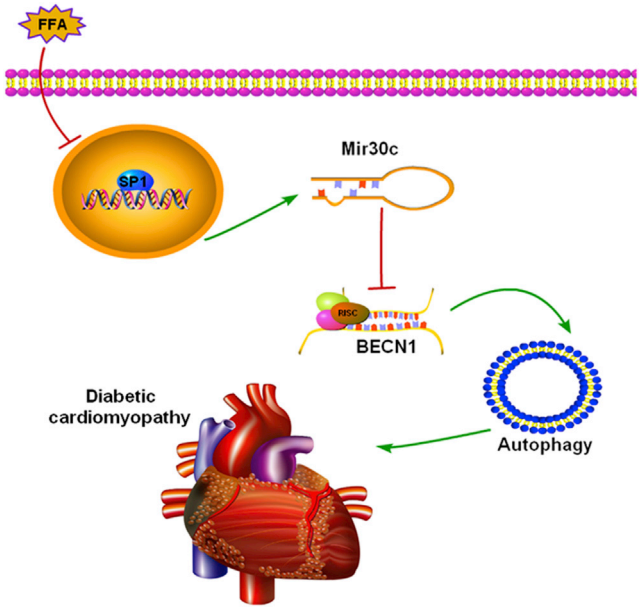

Figure 7. The Roles of *Mir30c* and Autophagy in Diabetic Cardiomyopathy
Our results show that in db/db hearts, lipotoxicity from increased levels of free fatty acids (FFAs) downregulates SP1 in the nucleus. This leads to less *Mir30c* being transcribed, which results in increased levels of BECN1. More BEC1 leads to more autophagy, which contributes to the pathology of diabetic cardiomyopathy in an undetermined manner.

generally abnormal in type 2 diabetes,[23] perturbed FFA levels may be the major reason behind the marked depletion of *Mir30c* in the myocardium of diabetes patients, providing a new perspective on the impact of lipotoxicity on diabetic hearts.

Although autophagy is conventionally considered to be a cell-protective mechanism,[24] it is also known as type II cell death, since cell death may occur as a result of excessive autophagy.[10, 17] Increasing evidence has demonstrated altered autophagy in various heart diseases,[9, 25] but its role in the heart remains unclear. Early reports indicated that low-level constitutive autophagy in the heart under baseline normal conditions is important for the maintenance of cardiomyocyte size, global cardiac structure, and cell function.[7] However, several studies have suggested that high levels of autophagy are not only associated with myocardial hypertrophy but also responsible for autophagic cell death in the failing heart,[26, 27] and the occurrence of autophagic cardiomyocytes is greater than the occurrence of apoptotic cells.[9] Therefore, autophagy in the heart may play different roles, beneficial or detrimental, in different cellular settings.[7] Regarding heart abnormalities in type 2 diabetes, Mellor et al. found that upregulated autophagy contributed to cardiac pathology in insulin resistance, suggesting an anti-survival role of autophagy in diabetic hearts.[11] Moreover, an obesogenic diet based on milk fat rather than lard induced gross and cellular hypertrophic cardiac dysfunction and increased autophagy in the hearts of mice.[28]

Under normal physiological conditions, glucose, lactate, and fatty acids are the main energy substrates that maintain cardiac performance. However, mitochondrial oxidative metabolism decreases and glycolysis becomes a significant source of energy in an overloaded heart. Insufficient ATP supply leads to starvation state, initiating autophagy,[29] which then can lead to cell death through excessive degradation of essential cellular components. In UMX7.1 hamsters, an animal model of dilated cardiomyopathy induced by the absence of *Sgcd* gene, cardiomyocyte loss induced by autophagic death was increased, which was confirmed by the presence of typical autophagic vacuoles.[25] However, chronic activation of AMP-activated protein kinase catalytic subunit alpha 2 by metformin prevented cardiomyopathy by upregulating autophagic activity in diabetic mice.[30] Considering the above, the role of autophagy in diabetes deserves further investigation, particularly with transgenic animal models, to evaluate autophagic flux in vivo.

Here, we have shown that high levels of FFAs and the subsequent loss of *Mir30c* are crucial for activation of autophagy in cardiomyocytes both in cultured H9c2 cells exposed to FFAs and in db/db mice. In contrast to previous investigations that principally explored the association between high glucose and autophagy,[30] we studied the role of autophagy in high-FFA conditions in diabetic hearts. We found that autophagy increase in response to high FFAs led to cardiac abnormalities in diabetes.

Although we have detected plasma expression of Mir30c in patients and involved cell lines and mouse models, there was no verification in humans of the role of Mir30c and relative proteins studied. Studies of the function of Mir30c in humans will provide information more directly to human disease.

In conclusion, we here demonstrated that cardiac abnormalities in db/db mice are associated with *Mir30c* depletion through autophagy regulation and that downregulation of SP1 results in reduced *Mir30c* levels. Our data suggest novel therapeutic targets for diabetic cardiomyopathy.

MATERIALS AND METHODS

Reagents

H9c2 and HEK293 cell lines were obtained from the American Type Culture Collection. Cell culture medium (high glucose-dulbecco's modified eagle medium [H-DMEM] and OPTI-MEM) and fetal bovine serum (FBS) were obtained from GIBCO (Life Technologies). Primers for miRNA qRT-PCR, miRNA mimics, siRNAs, and their controls were synthesized by RiboBio Corporation. Primers for mRNA real-time PCR were synthesized by BGI. Mouse monoclonal antibodies against BECN1 (catalog number sc-48381), ACTB (catalog number sc-47778), and SP1 (catalog number sc-420) were purchased from Santa Cruz Biotechnology. Rabbit polyclonal antibodies against LC3, ATG5, and ATG7 (Autophagy Antibody Sampler Kit, catalog number 4445) were purchased from Cell Signaling Technology. Mouse monoclonal antibody against ACTA1 (catalog number NBP1-97725) and rabbit polyclonal antibodies against ULK1 (Cat No: NB110-74844) and ATG14 (catalog number NBP2-36445) were purchased from Novus Biologicals. Rabbit polyclonal antibody

against SQSTM1 (catalog number A0682) was purchased from ABclonal. Pre-stained protein markers and DNA ladders were purchased from Fermentas (Thermo Fisher Scientific). Polyvinylidene difluoride (PVDF) membranes were obtained from Millipore (Merck KGaA). Baf A1, pepstatin A, and E64d were purchased from Cayman. All other reagents were obtained from Sigma-Aldrich Shanghai Trading Co., unless otherwise specified.

Human Tissue Samples

In accordance with the Declaration of Helsinki and with the approval of the Ethics Committee of Tongji Hospital, 28 healthy controls, 26 patients with diabetes, 22 patients with chronic heart failure, and 15 patients with both diabetes and chronic heart failure were enrolled in the study. All patients were admitted to the Cardiovascular Division of Tongji Hospital between January 2012 and January 2016. Fasting blood samples were collected via venous puncture after obtaining written informed consent. The clinical characteristics of the patients and control participants are listed in Table S1. After centrifugation, the plasma samples were transferred to RNase-free tubes and stored at −80°C until further analysis.

Animals

The animal study was approved by the Institutional Animal Research Committee of Tongji Medical College. For in vivo experiments, male db/db mice generated in C57BL/Ks background and control C57BL/Ks mice (Model Animal Research Center of Nanjing University) were used. All experiments were performed in accordance with the ARRIVE guidelines and NIH guidelines for animal welfare. All animals were maintained under a 12 hr light/12 hr dark photoperiod, with free access to water and food. We randomly divided the db/db mice into five groups (n = 8 in each group): control, rAAV-miR-random, rAAV-*Mir30c*, rAAV-anti-*Mir30c*, and rAAV-*Mir30c* + rAAV-BECN1. The mice were injected with the corresponding rAAVs via tail vein at 16 weeks of age. Echocardiographic analysis was performed under inhalation anesthesia with 2% isoflurane.[31] Mice were anesthetized with intraperitoneal injections of a ketamine (80 mg/kg) and xylazine (5 mg/kg) mixture before hemodynamic analyses.[32] To assess the adequacy of the anesthesia during hemodynamic examinations, parameters such as responsiveness, blood pressure, and respiratory and heart rates were monitored. The mice were killed by CO_2 inhalation. The rAAV-treated db/db and control mice were sacrificed at 24 weeks of age, and tissue samples were snap-frozen in liquid nitrogen or collected for paraffin embedding.

Isolation of Primary Cardiomyocytes

Cardiomyocytes (CMs) and non-cardiomyocytes (NCMs) were isolated from adult mice, as described previously.[33] Briefly, the left ventricles were harvested from perfused and digested hearts and dissected into small pieces for dissociation in transfer buffer. After filtering the cell solution, the cells were settled by sedimentation for several minutes in Falcon tubes. Cell pellets and supernatants were transferred to individual Falcon tubes for further separation. Cell pellets were re-suspended in transfer buffer and settled by repeated precipitation. After a second precipitation, the cell pellets were examined for typical rod-shaped cell morphology before RNA extraction to verify the expression of CM markers. The initial supernatant was first centrifuged at 50 × *g* (3 min) and then at 300 × *g* (5 min) before verification of the pelleted cell NCM identity by qRT-PCR assessment of fibroblast and CM markers.[34]

Western Blot Analysis

Western blotting was performed using specific antibodies (primary antibody dilution 1:1,000), as described previously.[35] Individual band intensities were analyzed by densitometry using ImageJ (NIH software).

Autophagic Flux Analysis

Cells were treated with Ad-mRFP-GFP-LC3 (catalog number HB-AP2100001, Hanbio) for 48 hr, according to the manufacturer's instructions and were then assessed for green (GFP) or red (mRFP) fluorescence. Autophagosomes were observed as yellow puncta and autolysosomes were observed as red puncta in merged images. Autophagic flux was measured as a percent increase in red puncta in the merged images, as described previously.[36]

Cell Culture and Treatment

For in vitro experiments, H9c2 cells were routinely maintained in H-DMEM supplemented with 10% FBS at 37°C in an atmosphere of 5% CO_2. The cells were cultured in six-well plates and grown to ∼60%–70% confluence before transfection. Transfection with miRNA mimics (100 nM), siRNAs (100 nM), and relative controls (100 nM) was performed with Lipofectamine 2000 (LF2K for short, Invitrogen, Life Technologies Corporation), according to the manufacturer's recommendations. For high-FFA stimulation, H9c2 cells were treated with palmitate (1 mM or 2 mM) as previously described, for 48 h.[37] Baf A1 (10 nM), pepstatin A (10 μg/mL), and E64d (10 μg/mL) were administered for 2 hr. For luciferase assays, HEK293 cells were cultured in H-DMEM supplemented with 10% FBS and co-transfected in 24-well plates using Lipofectamine 2000 with 200 ng of the appropriate luciferase pMIR construct and 10 ng pRL-TK plasmid (Promega). In addition, *Mir30c* mimics or si-SP1, and the corresponding controls were used (final concentration 100 nM) to co-transfect with reporter plasmids in HEK293 cells.

Real-Time qPCR

Total RNA was extracted from animal hearts or H9c2 cells using a TRIzol Reagent Kit (Invitrogen, Life Technologies) and reverse-transcribed with a specific RT primer (RiboBio) using an EasyScript First-Strand cDNA Synthesis SuperMix (Transgen Biotech Corporation). Real-time qPCR was performed with specific primers according to the manufacturer's protocol (RiboBio). U6 small nuclear RNA expression was used as an internal standard, and miRNA expression was normalized to U6. The mRNA primers are listed in Table S5. Each reaction was performed in triplicate, and data analysis was performed by $2^{-\Delta\Delta Ct}$ method as described previously.[38]

miRNA Target Prediction

Bioinformatics prediction websites TargetScan (http://www.targetscan.org/) and miRBase (http://www.mirbase.org/) were used for *Mir30c*

target prediction. To predict transcription factor binding sites in gene promoter regions, the program Alibaba 2.0 (http://gene-regulation.com/pub/programs.html.) was used. The National Center for Biotechnology Information's (https://www.ncbi.nlm.nih.gov/) BLAST program was used for analyses of the sequences of potential target genes.

Construction of Luciferase Reporter Plasmids

The full-length sequence of the human BECN1 3′ UTR was amplified by PCR using the primers forward 5′-GAGCTCACTCTGAGG AGCAGTGGA-3′ and reverse 5′-TTCGAAATCTGGGTGACCTT GACT-3′ and was then mutated using Fast Mutagenesis System (Transgen Biotech Corporation), according to the manufacturer's instructions. To construct luciferase reporter plasmids, the 3′ UTR and mutant 3′ UTR of BECN1 were inserted into pMIR-REPORT luciferase vector (Ambion).

Based on the predictions, the 5′ promoter region (∼1,000 to 0 bp) of *Mir30c* was cloned into the tpGL3 luciferase reporter vector (Promega) following the manufacturer's protocol.

Dual Luciferase Assays

Luciferase activity was analyzed 48 hr after transfection using a dual-luciferase reporter assay system (Promega), according to the manufacturer's recommendations. The activity of *Renilla* luciferase was used to normalize the transfection efficiency and the internally controlled firefly luciferase activity.

Cell Survival Assays

Cell-Counting Kit 8 (CCK8) assays were performed to assess cell survival as described previously.[39]

BrdU Incorporation Assays

A bromodeoxyuridine (BrdU) immunolabeling assay was performed using a nonisotopic immunoassay kit to quantify BrdU incorporation into newly synthesized DNA of actively proliferating cells, according to the manufacturer's instructions (Calbiochem, EMD Chemicals), as described previously.[40]

Annexin V/Propidium Iodide Assays

Treated cells were harvested, resuspended in binding buffer, incubated with fluorescein isothiocyanate (FITC)-conjugated Annexin V and propidium iodide (PI; Annexin V-FITC Apoptosis Detection Kit, BD) according to the manufacturer's protocol, and then analyzed with FACStar Plus flow cytometer (BD). To exclude necrotic cells, only Annexin-V-positive and PI-negative cells (early apoptotic cells) were counted.

Caspase-3 Activity Assays

Caspase-3 activity was measured using a colorimetric assay kit according to the manufacturer's instructions (R&D Systems).

Construction and Preparation of Recombinant Adeno-Associated Viruses

rAAV vectors (type 9) were used to express *Mir30c*, BECN1, and the appropriate controls in heart tissues in vivo. The rAAV-9 system was a kind gift from Dr. Xiao Xiao (University of North Carolina at Chapel Hill). Three plasmids used to co-transfect HEK293 cells were purified as described previously.[41] To construct rAAV vectors carrying *Mir30c*, anti-*Mir30c*, or miR-random, the respective complementary single oligonucleotide strands were synthesized (BGI). After annealing, double-stranded DNA fragments were ligated with rAAV vectors. To construct rAAV vectors carrying BECN1, full-length BECN1 sequence was PCR-amplified using specific primers (forward: 5′-CGCGGAT CCTCCCGAGGTGAAGAGCAT-3′, reverse: 5′-AAGGAAAAAAGC GGCCGCAAAAGCCTTTAAGGCAAA-3′). The amplified products were then cloned into rAAV vectors. The rAAVs were aliquoted and stored at −80°C until use.

Electron Microscopy

Heart samples were fixed in 2% glutaraldehyde in PBS and electron microscopy analysis was performed using a Tecnai G2 12 transmission electron microscope (FEI). Autophagosomes were counted in ten images from different fields (five or more). The characteristic smooth double-membrane structures completely surrounding compressed mitochondria or membrane-bound electron-dense material were identified as autophagosomes.[42]

Histological Analysis and CM Size Determination

After sacrifice, mouse hearts were collected for paraffin embedding and sectioned. After H&E staining, CM sizes were determined by morphology. Masson and Sirius red staining was performed to assess cardiac fibrosis. For histological analysis, the tissue sections were stained with specific antibodies (primary antibody dilution 1:200) and secondary antibodies, visualized by light microscopy, photographed (200×), and analyzed by ImagePro software.

TUNEL Assays

Cardiac apoptosis was determined using TUNEL staining, according to the manufacturer's instructions (R&D Systems). Images were acquired using an inverted microscope (TE 2000; Nikon) equipped with digital imaging camera. For each slide, ten high-power field images were captured.

EdU Incorporation Assays

EdU (50 mg/kg) was subcutaneously injected into mice every day for 3 days before sacrifice, as described previously.[34] EdU staining was then performed according to manufacturer's instructions (RiboBio). For each slide, ten high-power field images were captured.

Echocardiography and In Vivo Hemodynamics

After anesthetization, echocardiographic analysis was performed to determine cardiac function of 24-week-old mice using a high-resolution imaging system with a 30-MHz high frequency scanhead (VisualSonics Vevo770, VisualSonics), as described previously.[35] Briefly, a parasternal long-axis B-mode image was acquired with appropriate positioning of the scan head so that the maximum LV length could be identified. Then a clockwise 90° rotation at the papillary muscle level depicted the parasternal short-axis view. From this view, an M-mode cursor was positioned perpendicular to the anterior and

posterior walls of the left ventricle, and M-mode image loops were obtained for measurement of wall thickness and chamber dimensions. Each of these captured image loops included 11 to 20 cardiac cycles, and data were averages from at least three cycles per loop.

LVEF was calculated as follows: LVEF = (left ventricular end-diastolic volume [LVEDV] − left ventricular end-systolic volume [LVESV])/LVEDV × 100%. FS was calculated as follows: FS% = (left ventricular end diastolic dimension [LVDd] − left ventricular end systolic dimensions [LVDs])/LVDd × 100%.

Mouse hemodynamics were assessed as previously described.[35] Briefly, a catheter manometer (Millar 1.4F, SPR 835, Millar Instruments) was inserted in the right carotid artery and advanced into the left ventricle to measure instantaneous intraventricular pressure and volume. After stabilization, steady-state measurements were recorded. PVAN software (Millar Instruments) was used to perform the cardiac pressure-volume analysis. All data were averages of at least five measurements, and each measurement concluded at least ten successive loops. Global systolic function was measured as the peak instantaneous rate of the LV pressure increase and decline (dp/dt max, dp/dt min).

ChIP Assays

ChIP assays were carried out according to the manufacturer's protocol for the ChIP assay kit (Beyotime), as described previously.[43]

Statistical Analysis

The data are presented as mean ± SEM or mean ± SD. Student's t tests and ANOVAs were performed to identify statistically significant differences between treatment groups, as appropriate. In all cases, $p < 0.05$ was considered statistically significant.

SUPPLEMENTAL INFORMATION

Supplemental Information includes six figures and five tables and can be found with this article online at http://dx.doi.org/10.1016/j.omtn.2017.03.005.

AUTHOR CONTRIBUTIONS

All authors have approved this manuscript and its contents, and they are aware of the responsibilities connected with authorship. C.C. and S.Y. designed and performed the study, and analyzed the data; H.L., W.G., Z.Y., Y.Z., M.Y., and J.F. participated in performing the study; D.W.W. designed and organized the study.

ACKNOWLEDGMENTS

We thank colleagues in Dr. Wang's group for providing technical help and stimulating discussion during the course of this investigation.
This work was supported by the National Nature Science Foundation of China (grants 91439203, 31130031, 31571197, and 31400997) and the National 973 Program (grants 2012CB518004 and 2012CB517801).

REFERENCES

1. Rubler, S., Dlugash, J., Yuceoglu, Y.Z., Kumral, T., Branwood, A.W., and Grishman, A. (1972). New type of cardiomyopathy associated with diabetic glomerulosclerosis. Am. J. Cardiol. *30*, 595–602.
2. Boudina, S., and Abel, E.D. (2007). Diabetic cardiomyopathy revisited. Circulation *115*, 3213–3223.
3. Belke, D.D., Larsen, T.S., Gibbs, E.M., and Severson, D.L. (2000). Altered metabolism causes cardiac dysfunction in perfused hearts from diabetic (db/db) mice. Am. J. Physiol. Endocrinol. Metab. *279*, E1104–E1113.
4. Boudina, S., Bugger, H., Sena, S., O'Neill, B.T., Zaha, V.G., Ilkun, O., Wright, J.J., Mazumder, P.K., Palfreyman, E., Tidwell, T.J., et al. (2009). Contribution of impaired myocardial insulin signaling to mitochondrial dysfunction and oxidative stress in the heart. Circulation *119*, 1272–1283.
5. Boudina, S., Sena, S., O'Neill, B.T., Tathireddy, P., Young, M.E., and Abel, E.D. (2005). Reduced mitochondrial oxidative capacity and increased mitochondrial uncoupling impair myocardial energetics in obesity. Circulation *112*, 2686–2695.
6. Pereira, L., Matthes, J., Schuster, I., Valdivia, H.H., Herzig, S., Richard, S., and Gómez, A.M. (2006). Mechanisms of [Ca2+]i transient decrease in cardiomyopathy of db/db type 2 diabetic mice. Diabetes *55*, 608–615.
7. Nakai, A., Yamaguchi, O., Takeda, T., Higuchi, Y., Hikoso, S., Taniike, M., Omiya, S., Mizote, I., Matsumura, Y., Asahi, M., et al. (2007). The role of autophagy in cardiomyocytes in the basal state and in response to hemodynamic stress. Nat. Med. *13*, 619–624.
8. Levine, B., and Klionsky, D.J. (2004). Development by self-digestion: molecular mechanisms and biological functions of autophagy. Dev. Cell *6*, 463–477.
9. Kostin, S., Pool, L., Elsässer, A., Hein, S., Drexler, H.C., Arnon, E., Hayakawa, Y., Zimmermann, R., Bauer, E., Klövekorn, W.P., and Schaper, J. (2003). Myocytes die by multiple mechanisms in failing human hearts. Circ. Res. *92*, 715–724.
10. Baehrecke, E.H. (2005). Autophagy: dual roles in life and death? Nat. Rev. Mol. Cell Biol. *6*, 505–510.
11. Mellor, K.M., Bell, J.R., Young, M.J., Ritchie, R.H., and Delbridge, L.M. (2011). Myocardial autophagy activation and suppressed survival signaling is associated with insulin resistance in fructose-fed mice. J. Mol. Cell. Cardiol. *50*, 1035–1043.
12. Kim, V.N. (2005). MicroRNA biogenesis: coordinated cropping and dicing. Nat. Rev. Mol. Cell Biol. *6*, 376–385.
13. Wightman, B., Ha, I., and Ruvkun, G. (1993). Posttranscriptional regulation of the heterochronic gene lin-14 by lin-4 mediates temporal pattern formation in C. elegans. Cell *75*, 855–862.
14. van Rooij, E., Sutherland, L.B., Liu, N., Williams, A.H., McAnally, J., Gerard, R.D., Richardson, J.A., and Olson, E.N. (2006). A signature pattern of stress-responsive microRNAs that can evoke cardiac hypertrophy and heart failure. Proc. Natl. Acad. Sci. USA *103*, 18255–18260.
15. Goedeke, L., Rotllan, N., Canfrán-Duque, A., Aranda, J.F., Ramírez, C.M., Araldi, E., Lin, C.S., Anderson, N.N., Wagschal, A., de Cabo, R., et al. (2015). MicroRNA-148a regulates LDL receptor and ABCA1 expression to control circulating lipoprotein levels. Nat. Med. *21*, 1280–1289.
16. Shah, M.S., and Brownlee, M. (2016). Molecular and cellular mechanisms of cardiovascular disorders in diabetes. Circ. Res. *118*, 1808–1829.
17. Clarke, P.G. (1990). Developmental cell death: morphological diversity and multiple mechanisms. Anat. Embryol. (Berl.) *181*, 195–213.
18. Zhu, H., Wu, H., Liu, X., Li, B., Chen, Y., Ren, X., Liu, C.G., and Yang, J.M. (2009). Regulation of autophagy by a beclin 1-targeted microRNA, miR-30a, in cancer cells. Autophagy *5*, 816–823.
19. Pan, W., Zhong, Y., Cheng, C., Liu, B., Wang, L., Li, A., Xiong, L., and Liu, S. (2013). MiR-30-regulated autophagy mediates angiotensin II-induced myocardial hypertrophy. PLoS ONE *8*, e53950.
20. Duisters, R.F., Tijsen, A.J., Schroen, B., Leenders, J.J., Lentink, V., van der Made, I., Herias, V., van Leeuwen, R.E., Schellings, M.W., Barenbrug, P., et al. (2009). miR-133 and miR-30 regulate connective tissue growth factor: implications for a role of microRNAs in myocardial matrix remodeling. Circ. Res. *104*, 170–178.

21. Aasum, E., Hafstad, A.D., Severson, D.L., and Larsen, T.S. (2003). Age-dependent changes in metabolism, contractile function, and ischemic sensitivity in hearts from db/db mice. Diabetes *52*, 434–441.

22. Zhou, Y.T., Grayburn, P., Karim, A., Shimabukuro, M., Higa, M., Baetens, D., Orci, L., and Unger, R.H. (2000). Lipotoxic heart disease in obese rats: implications for human obesity. Proc. Natl. Acad. Sci. USA *97*, 1784–1789.

23. Grundy, S.M., Benjamin, I.J., Burke, G.L., Chait, A., Eckel, R.H., Howard, B.V., Mitch, W., Smith, S.C., Jr., and Sowers, J.R. (1999). Diabetes and cardiovascular disease: a statement for healthcare professionals from the American Heart Association. Circulation *100*, 1134–1146.

24. Kuma, A., Hatano, M., Matsui, M., Yamamoto, A., Nakaya, H., Yoshimori, T., Ohsumi, Y., Tokuhisa, T., and Mizushima, N. (2004). The role of autophagy during the early neonatal starvation period. Nature *432*, 1032–1036.

25. Miyata, S., Takemura, G., Kawase, Y., Li, Y., Okada, H., Maruyama, R., Ushikoshi, H., Esaki, M., Kanamori, H., Li, L., et al. (2006). Autophagic cardiomyocyte death in cardiomyopathic hamsters and its prevention by granulocyte colony-stimulating factor. Am. J. Pathol. *168*, 386–397.

26. Hein, S., Arnon, E., Kostin, S., Schönburg, M., Elsässer, A., Polyakova, V., Bauer, E.P., Klövekorn, W.P., and Schaper, J. (2003). Progression from compensated hypertrophy to failure in the pressure-overloaded human heart: structural deterioration and compensatory mechanisms. Circulation *107*, 984–991.

27. Takemura, G., Miyata, S., Kawase, Y., Okada, H., Maruyama, R., and Fujiwara, H. (2006). Autophagic degeneration and death of cardiomyocytes in heart failure. Autophagy *2*, 212–214.

28. Russo, S.B., Baicu, C.F., Van Laer, A., Geng, T., Kasiganesan, H., Zile, M.R., and Cowart, L.A. (2012). Ceramide synthase 5 mediates lipid-induced autophagy and hypertrophy in cardiomyocytes. J. Clin. Invest. *122*, 3919–3930.

29. Kanamori, H., Takemura, G., Goto, K., Tsujimoto, A., Mikami, A., Ogino, A., et al. (2015). Autophagic adaptations in diabetic cardiomyopathy differ between type 1 and type 2 diabetes. Autophagy *11*, 1146–1160.

30. Xie, Z., Lau, K., Eby, B., Lozano, P., He, C., Pennington, B., Li, H., Rathi, S., Dong, Y., Tian, R., et al. (2011). Improvement of cardiac functions by chronic metformin treatment is associated with enhanced cardiac autophagy in diabetic OVE26 mice. Diabetes *60*, 1770–1778.

31. Matsuda, Y., Ohsaka, K., Yamamoto, H., Natsume, K., Hirabayashi, S., Kounoike, M., and Inoue, M. (2007). Comparison of newly developed inhalation anesthesia system and intraperitoneal anesthesia on the hemodynamic state in mice. Biol. Pharm. Bull. *30*, 1716–1720.

32. Pacher, P., Nagayama, T., Mukhopadhyay, P., Bátkai, S., and Kass, D.A. (2008). Measurement of cardiac function using pressure-volume conductance catheter technique in mice and rats. Nat. Protoc. *3*, 1422–1434.

33. Graham, E.L., Balla, C., Franchino, H., Melman, Y., del Monte, F., and Das, S. (2013). Isolation, culture, and functional characterization of adult mouse cardiomyoctyes. J. Vis. Exp. *24*, e50289.

34. Liu, X., Xiao, J., Zhu, H., Wei, X., Platt, C., Damilano, F., Xiao, C., Bezzerides, V., Boström, P., Che, L., et al. (2015). miR-222 is necessary for exercise-induced cardiac growth and protects against pathological cardiac remodeling. Cell Metab. *21*, 584–595.

35. Yang, S., Chen, C., Wang, H., Rao, X., Wang, F., Duan, Q., Chen, F., Long, G., Gong, W., Zou, M.H., and Wang, D.W. (2012). Protective effects of Acyl-coA thioesterase 1 on diabetic heart via PPARα/PGC1α signaling. PLoS ONE *7*, e50376.

36. Klionsky, D.J., Abdelmohsen, K., Abe, A., Abedin, M.J., Abeliovich, H., Acevedo Arozena, A., Adachi, H., Adams, C.M., Adams, P.D., Adeli, K., et al. (2016). Guidelines for the use and interpretation of assays for monitoring autophagy (3rd edition). Autophagy *12*, 1–222.

37. Wang, H.J., Lee, E.Y., Han, S.J., Kim, S.H., Lee, B.W., Ahn, C.W., Cha, B.S., and Lee, H.C. (2012). Dual pathways of p53 mediated glucolipotoxicity-induced apoptosis of rat cardiomyoblast cell: activation of p53 proapoptosis and inhibition of Nrf2-NQO1 antiapoptosis. Metabolism *61*, 496–503.

38. Long, G., Wang, F., Duan, Q., Yang, S., Chen, F., Gong, W., Yang, X., Wang, Y., Chen, C., and Wang, D.W. (2012). Circulating miR-30a, miR-195 and let-7b associated with acute myocardial infarction. PLoS ONE *7*, e50926.

39. Zhang, Y.W., Niu, J., Lu, X., Yang, Y.X., Zhao, H.W., He, X., Yin, G.W., Wu, J.D., Yan, D.L., Sun, J.F., et al. (2013). Multi-target lentivirus specific to hepatocellular carcinoma: in vitro and in vivo studies. J. Hepatol. *58*, 502–508.

40. Chen, C., Wang, Y., Yang, S., Li, H., Zhao, G., Wang, F., Yang, L., and Wang, D.W. (2015). MiR-320a contributes to atherogenesis by augmenting multiple risk factors and down-regulating SRF. J. Cell. Mol. Med. *19*, 970–985.

41. Jiang, J.G., Ning, Y.G., Chen, C., Ma, D., Liu, Z.J., Yang, S., Zhou, J., Xiao, X., Zhang, X.A., Edin, M.L., et al. (2007). Cytochrome p450 epoxygenase promotes human cancer metastasis. Cancer Res. *67*, 6665–6674.

42. Klionsky, D.J., Abdalla, F.C., Abeliovich, H., Abraham, R.T., Acevedo-Arozena, A., Adeli, K., Agholme, L., Agnello, M., Agostinis, P., Aguirre-Ghiso, J.A., et al. (2012). Guidelines for the use and interpretation of assays for monitoring autophagy. Autophagy *8*, 445–544.

43. Wang, G., Cao, X., Lai, S., Luo, X., Feng, Y., Wu, J., Ning, Q., Xia, X., Wang, J., Gong, J., and Hu, J. (2015). Altered p53 regulation of miR-148b and p55PIK contributes to tumor progression in colorectal cancer. Oncogene *34*, 912–921.

OMTN, Volume *7*

Supplemental Information

Mir30c Is Involved in Diabetic Cardiomyopathy through Regulation of Cardiac Autophagy via BECN1

Chen Chen, Shenglan Yang, Huaping Li, Zhongwei Yin, Jiahui Fan, Yanru Zhao, Wei Gong, Mengwen Yan, and Dao Wen Wang

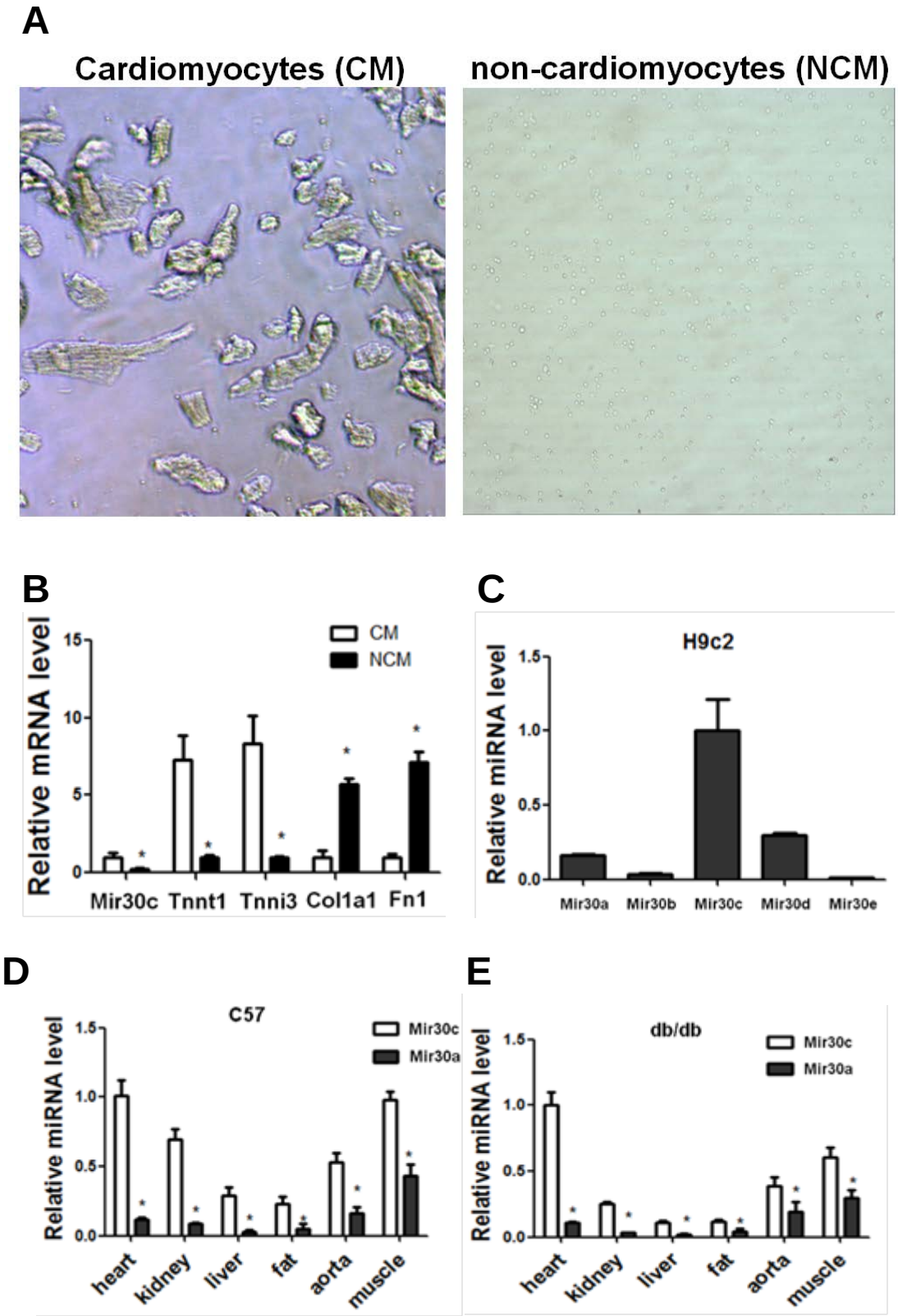

Supplemental Figure 1. Mir30c distribution and expression in various organs. A, Morphology of isolated primary cells. The small circles in the NCM image represent fibroblasts. B to E, Relative gene expression, as determined

by qRT-PCR. B, Relative expression of CM and NCM markers in isolated primary cells. *$p<0.05$ vs. CMs. C, Relative expression of Mir30 family miRNAs in H9c2 cells. D, Relative expression of Mir30a and Mir30c in various organs of C57BL/Ks mice. *$p<0.05$ vs. Mir30c. E, Relative expression of Mir30a and Mir30c in various organs of db/db mice. *$p<0.05$ vs. Mir30c. Data are expressed as mean±SEM, n=8. Data are representative of three independent experiments.

A

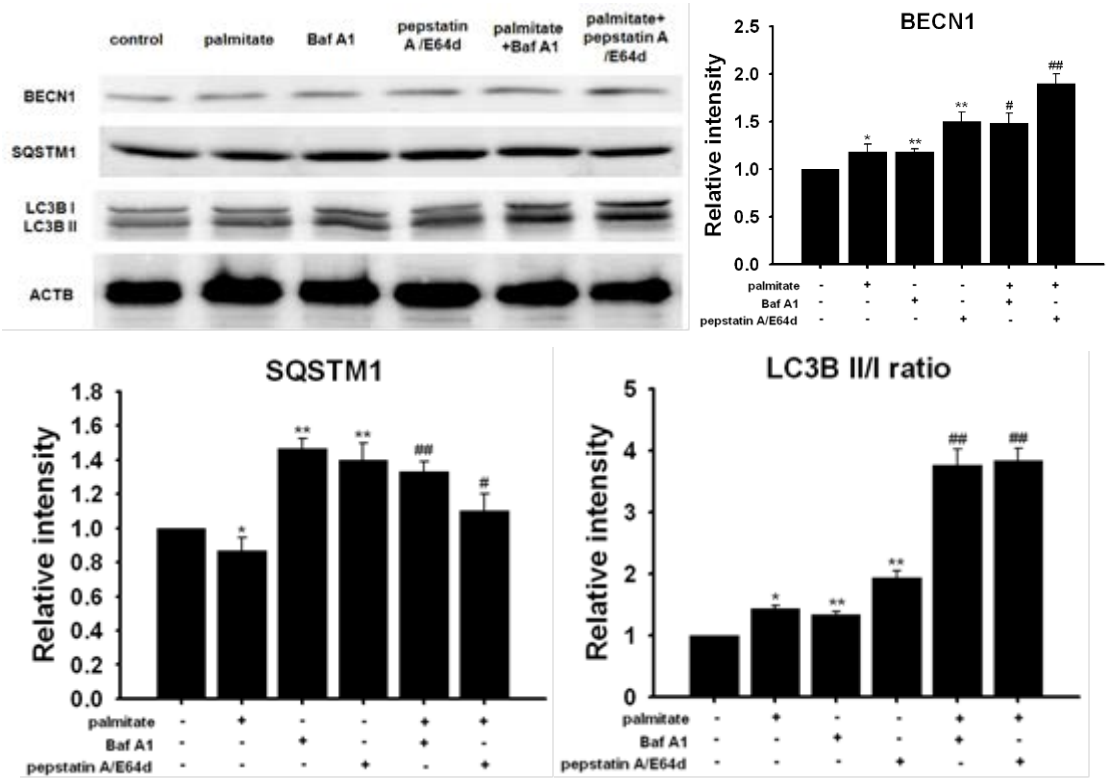
control
palmitate
Baf A1
pepstatin A /E64d
palmitate +Baf A1
palmitate+ pepstatin A /E64d
BECN1
SQSTM1
LC3B I
LC3B II
ACTB
BECN1
Relative intensity
SQSTM1
Relative intensity
LC3B II/I ratio
Relative intensity
palmitate
Baf A1
pepstatin A/E64d

B

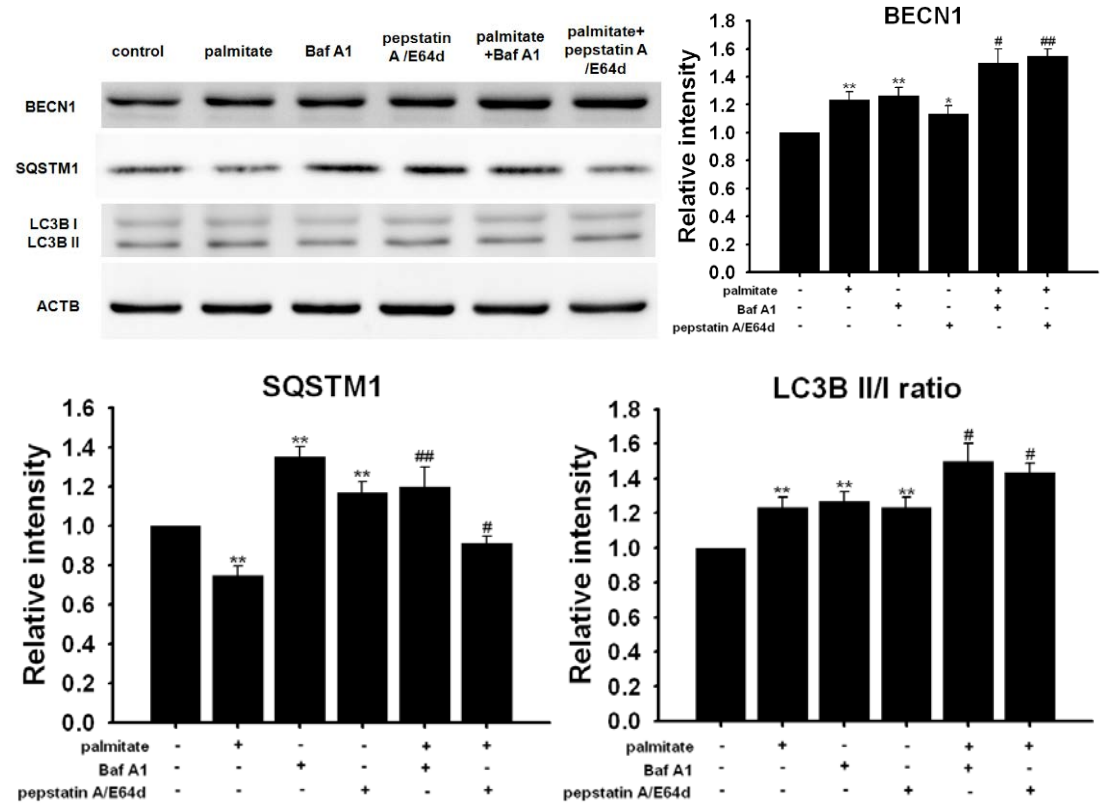
control
palmitate
Baf A1
pepstatin A /E64d
palmitate +Baf A1
palmitate+ pepstatin A /E64d
BECN1
SQSTM1
LC3B I
LC3B II
ACTB
BECN1
Relative intensity
SQSTM1
Relative intensity
LC3B II/I ratio
Relative intensity
palmitate
Baf A1
pepstatin A/E64d

Supplemental Figure 2. High FFA concentrations enhance autophagy in cultured H9c2 cardiac cells. H9c2 cells were analyzed after treatment with palmitate (1 mM) for 48 h. A, Bafilomycin A1 (Baf A1, 10 nM), or pepstatin A (10 μg/mL) and E64d (10 μg/mL) were added 4 h before harvesting. B, Bafilomycin A1 (Baf A1, 10 nM), or pepstatin A (10 μg/mL) and E64d (10 μg/mL) were added 12 h before harvesting. Data are expressed as mean±SEM. *$p<0.05$ vs. control, **$p<0.01$ vs. control, $^{\#}p<0.05$ vs. palmitate, $^{\#\#}p<0.01$ vs. palmitate. Data are representative of three independent experiments.

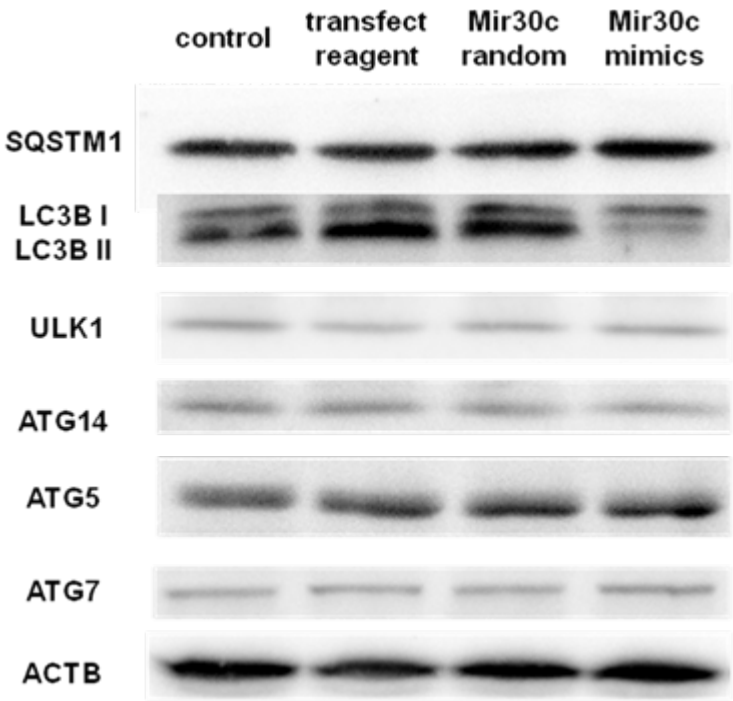

Supplemental Figure 3. The effect of Mir30c on the abundance of autophagy-associated proteins. Levels of autophagy-associated proteins were detected in H9c2 cells by western blotting. ACTB was used as an internal control. Experimental details can be found in Materials and Methods.

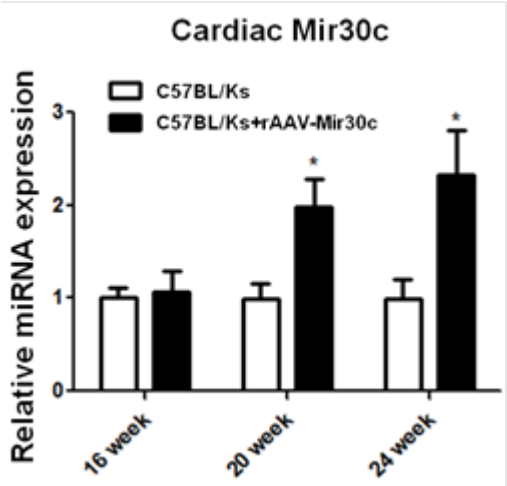

Supplemental Figure 4. The expression of *Mir30c* in C57BL/Ks control mice of different ages. The rAAVs were injected via the tail vein of 16-week-old animals, and cardiac *Mir30c* expression was determined every 4 weeks by qRT-PCR. U6 was used as an internal control. *$p<0.05$ vs. untreated control at the same time point. Data are expressed as means±SEM (n=8). They are representative of three independent experiments.

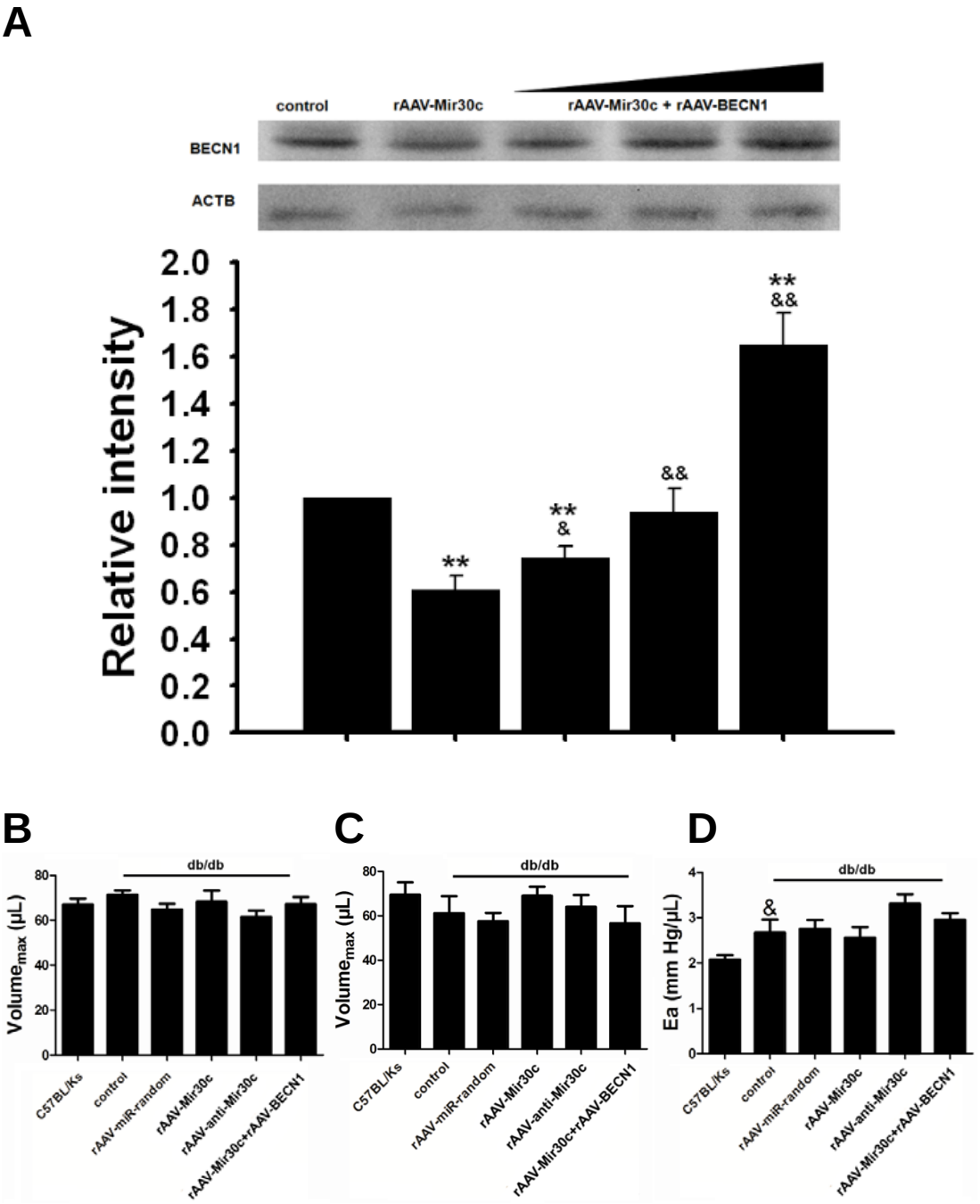

Supplemental Figure 5. BECN1 rescues cardiac function in db/db mice. A, Three different doses of BECN1 (0.5×10^{11} virion particles, 1×10^{11} virion particles, or 2×10^{11} virion particles) rescued cardiac BECN1 expression in db/db mice, as determined by western blotting. **$p<0.01$ vs. control, $^{\#}p<0.05$ vs. rAAV-Mir30c, $^{\#\#}p<0.01$ versus rAAV-Mir30c. B, Volume$_{max}$, determined by hemodynamic analyses. C, Volume$_{max}$, assessed by echocardiography. D, Ea,

determined by hemodynamic analyses. $^{\&}p<0.05$ vs. C57BL/Ks. Data are expressed as mean±SEM (n=8). They are representative of three independent experiments.

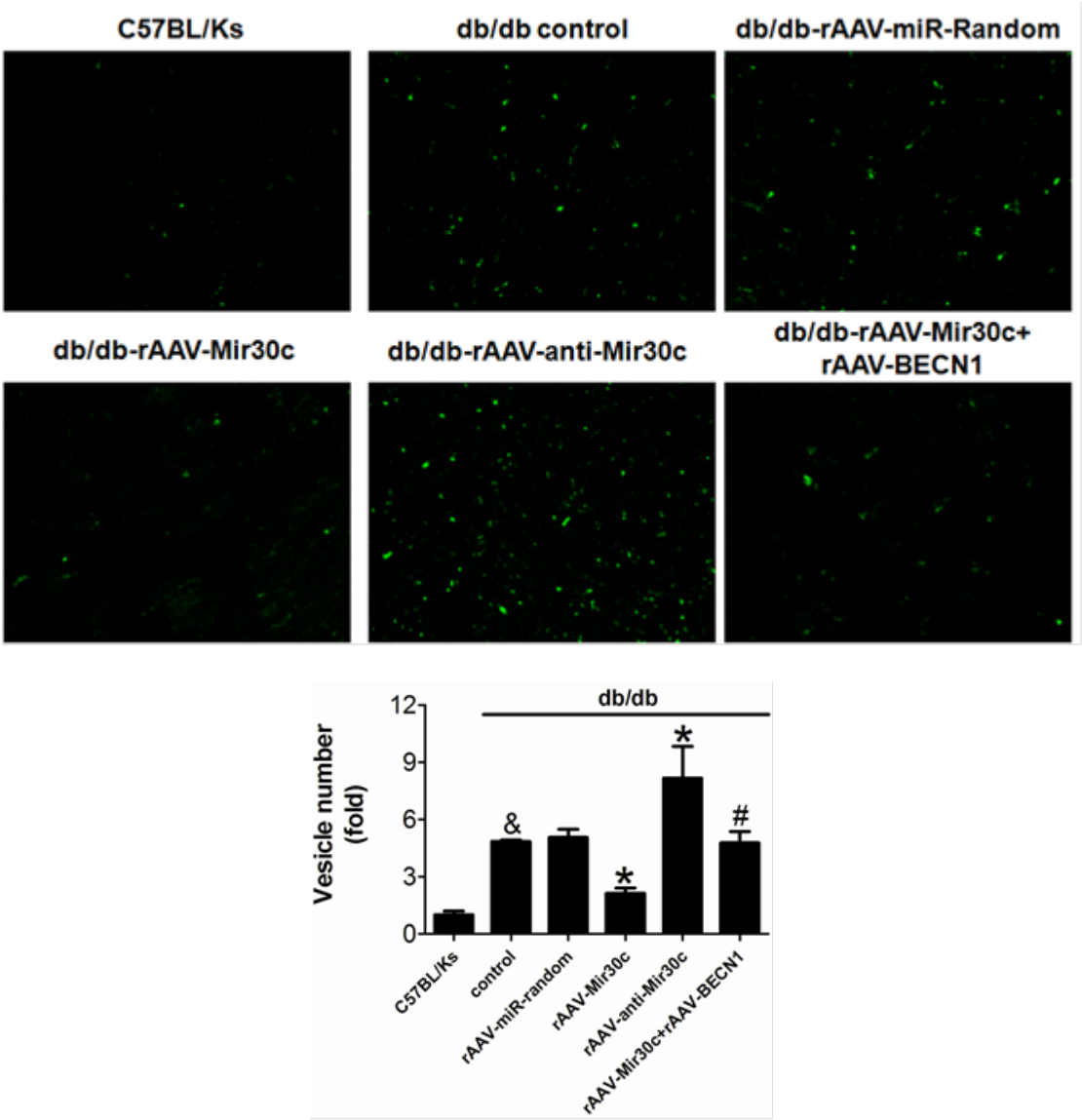

Supplemental Figure 6. Autophagosome formation in db/db mice. db/db mice were treated with different rAAVs for 4 weeks and injected with pCMV-LC3-GFP via their tail vein 1 week before sacrifice subsequently. GFP-LC3 expression in the heart was analyzed by confocal microscopy (upper panels; 600× magnification). Autophagosomes were quantified by counting GFP-LC3–positive dots and normalizing for cross-sectional area (lower panel). Data are expressed as mean±SEM (n=5). $^{\&}p<0.05$ vs. C57BL/Ks, $^{*}p<0.05$ vs. db/db control, $^{\#}p<0.05$ vs. db/db rAAV-*Mir30c*. Data are representative of three independent experiments.

Supplemental Table 1. Baseline clinical characteristics of controls and patients

Characteristic[a]	**Control (n=28)**	**Diabetes (n=26)**	**Chronic heart failure (n=22)**	**Diabetes combined with chronic heart failure (n=15)**
Male/female (n/n)	14/14	9/17	14/8	10/5
Age (years)	56.6±1.46	61.6±1.85	58.0±3.44	60.0±3.03
SBP (mmHg)	125±3	147±5*	123±5	138±6[#]
DBP (mmHg)	77±2	84±4	77±3	82±6
Cr (mmol/L)	69.9±2.3	64.1±4.6	95.1±6.1*	86.1±6.8*
BUN (mmol/L)	5.00±0.25	6.46±0.45*	8.25±0.75*	8.90±1.10*
Fasting glucose (mmol/L)	5.18±0.10	14.2±1.31*	6.17±0.25*	10.0±0.33*[#]
TG (mmol/L)	1.35±0.17	1.72±0.19	1.19±0.11	1.32±0.17
TC (mmol/L)	4.02±0.13	3.86±0.14	3.86±0.18	4.01±0.33
HDL (mmol/L)	1.10±0.06	0.93±0.05	0.95±0.06	0.80±0.10*
LDL (mmol/L)	2.44±0.12	2.21±0.12	2.49±0.16	2.64±0.31
NT-proBNP (ng/L)	66±10	621±202*	4715±915*	5574±1647*
EF (%)	65.1±1.6	65.6±1.0	36.5±2.6*	35.2±2.6*

[a] BMI, Body mass index; SBP, systolic blood pressure; DBP, diastolic blood pressure; Cr, creatinine; BUN, blood urea nitrogen; TG, Triglyceride; TC, total cholesterol; HDL, high-density lipoprotein; LDL, low-density lipoprotein; NT-proBNP, amino-terminal pro-brain natriuretic peptide; EF, ejection fraction. Data are presented as mean±SEM. *$p<0.05$ vs. control; [#]$p<0.05$ vs. chronic heart failure.

Supplemental Table 2. Hemodynamic variables of C57BL/Ks mice receiving different treatments[a]

Variable[b]	**Control (8)**	**rAAV-miR-Random (8)**	**rAAV-*Mir30c* (8)**	**rAAV-anti-*Mir30c* (8)**
HR (b.p.m.)	528±54	493±40	505±50	507±39
dP/dt_{max} (mmHg/s)	11,630±542	11,480±633	11,918±385	12,248±703
dP/dt_{min} (mmHg/s)	-10,833±1053	-11,204±726	-11,423±972	-11,504±355
P_{max} (mmHg)	107.8±4.8	107.6±3.4	104.6±3.7	108.4±3.6
P_{es} (mmHg)	94.3±5.6	92.2±1.9	94.8±4.6	94.3±4.6

[a] Data are expressed as mean±SD; numbers in parentheses represent numbers of mice/group; ANOVA test was performed, and $p<0.05$ was considered statistically significant. No significant differences were detected among the groups.

[b] HR, heart rate; P_{max}, maximum pressure; P_{es}, end-systolic pressure.

Supplemental Table 3. Echocardiographic characteristics of LV parameters in C57BL/Ks and db/db mice that received different treatments[a]

Characteristic[b]	**C57BL/Ks (8)**[c]	**db/db**				
		control (8)	**rAAV-miR-Random (8)**	**rAAV-*Mir30c* (8)**	**rAAV-anti-*Mir30c* (8)**	**rAAV-*Mir30c*+ rAAV-BECN1 (8)**
HR (b.p.m.)	502±5	450±13[&]	469±14	461±16	462±18	455±15
LVPWd (mm)	0.79±0.04	0.82±0.05	0.82±0.13	0.84±0.07	1.00±0.06	0.91±0.07
LVPWs (mm)	1.12±0.13	1.13±0.08	1.13±0.10	1.16±0.09	1.19±0.07	1.19±0.14
LVAWd (mm)	0.83±0.03	0.88±0.06	0.89±0.07	0.85±0.07	0.92±0.06	0.90±0.09
LVAWs (mm)	1.18±0.08	1.22±0.08	1.28±0.03	1.26±0.13	1.39±0.16	1.27±0.13
LVIDd (mm)	3.66±0.11	3.77±0.35	3.68±0.20	3.97±0.22	3.84±0.26	3.64±0.42
LVIDs (mm)	2.23±0.07	2.56±0.25[&]	2.49±0.18	2.45±0.12	2.85±0.25	2.48±0.35
LV Vold (μL)	56.72±3.84	61.14±13.29	57.56±7.45	69.04±9.09	64.02±10.74	56.63±15.50
LV Vols (μL)	16.80±1.41	23.88±5.63[&]	22.18±4.03	21.26±2.56	31.15±6.74	22.52±7.74

[a] Data are expressed as mean±SD; numbers in parentheses represent numbers of mice/group; Student's *t* test was performed and $p<0.05$ was considered statistically significant.

[b] HR, heart rate; LVPW, left ventricular posterior wall thickness; LVAW, Left ventricular anterior wall thickness; LVID, left ventricular internal dimension; LV Vol, left ventricular volume; s, end-systole; d, end-diastole.

[c] [&]$p<0.05$ vs. C57BL/Ks.

Supplemental Table 4. Hemodynamic variables of db/db mice receiving different treatments[a]

Variable[b]	**Control (8)**[c]	**rAAV-miR-Random (8)**	**rAAV-*Mir30c* (8)**	**rAAV-*Mir30c*+ rAAV-BECN1 3′-UTR WT (8)**	**rAAV-*Mir30c*+ rAAV-BECN1 3′-UTR mut (8)**	**rAAV-miR-Random +rAAV-BECN1 3′-UTR WT (8)**
HR (b.p.m.)	428±37	415±31	398±44	432±35	397±39	398±25
dP/dt_{max} (mmHg/s)	8302±418	8450±681	9581±696*	9121±326*	7856±546[&]	6269±422[#]
dP/dt_{min} (mmHg/s)	-6165±778	-6242±607	-7245±880*	-5922±968	-5195±392[&]	-5075±380
P_{max} (mmHg)	98.2±5.7	99.9±9.3	99.3±4.2	108.4±3.6[&]	103.4±5.2	96.8±4.2
P_{es} (mmHg)	85.3±8.7	91.2±9.0	93.9±6.9	88.5±1.8	96.3±9.5	92.4±8.9

[a] Data are expressed as mean±SD; numbers in parentheses represent numbers of mice/group. Student's *t* test was performed.

[b] HR, heart rate; P_{max}, maximum pressure; P_{es}, end-systolic pressure.

[c] *$p<0.05$ vs. control; [&]$p<0.05$ vs. rAAV-*Mir30c*; [#]$p<0.05$ vs. rAAV-miR-Random.

Supplemental Table 5. Real-time PCR primers

Gene	Forward	Reverse
Mouse Tnnt1	5′ TCGACCACCTGAATGAAGACC 3′	5′ TTCCTGCAGGTCGAACTTCTC 3′
Mouse Tnni3	5′ TCTATGACCTCCGTGGCAAGT 3′	5′ TCCTCCTTCTTCACCTGCTTG 3′
Mouse Col1a1	5′ CCGAGGTATGCTTGATCT 3′	5′ GACAGTCCAGTTCTTCATTG 3′
Mouse Fn1	5′ GTGTCTATGCTCTCAAGGA 3′	5′ CTAATAGTGATGGTGGTCTCT 3′
Mouse Sp1	5′ AACCTTCCTTGTCTTGGCTGAG 3′	5′ TCAGTTCCCTGGTAGAGAAGGC 3′
Mouse Gapdh	5′ GGTGAAGGTCGGTGTGAACG 3′	5′ CTCGCTCCTGGAAGATGGTG 3′
Rat Becn1	5′ GCCACAAGCATCTCATCTCAAA 3′	5′ AGCACGCCATGTATAGCAAAGA 3′
Rat Gapdh	5′ ACAGCAACAGGGTGGTGGAC 3′	5′ TTTGAGGGTGCAGCGAACTT 3′